UCRL-ID-104554
PATC-IR 89-05

MECHANICAL PROPERTIES OF ROCKS FROM PSA FLIGHT 1771 CRASH SITE

December 31, 1989

S. C. Blair, J. C. Chen, W. R. Ralph, D. W. Kuddle

Prepared for
U.S. Nuclear Regulatory Commission

DISCLAIMER

This work was supported by the United States Nuclear Regulatory Commission under a Memorandum of Understanding with the United States Department of Energy.

PATC-IR 89-05

MECHANICAL PROPERTIES OF ROCKS FROM PSA FLIGHT 1771 CRASH SITE

December 31, 1989

S. C. Blair, J. C. Chen, W. R. Ralph, D. W. Ruddle

Prepared for
U.S. Nuclear Regulatory Commission

ABSTRACT

Geotechnical properties of the near-surface rocks at the PSA Flight 1771 crash site have been determined from a variety of laboratory tests and measurements on cylindrical rock samples prepared from specimens derived from subsurface drill cores and from surface outcrop and "float" material. Pressure-volume tests to determine bulk modulus were conducted on specimens 2.54 cm (1 in.) and 5.08 cm (2 in.) in diameter at pressures up to 480 MPa. The uniaxial compressive strengths for both groups of samples were also measured. Results show that the uniaxial strength is proportional to the density of the intact rock samples. The uniaxial strength is also dependent on the sample orientation with respect to bedding planes. Triaxial compression tests were conducted on both groups of samples at pressures between 25 and 500 MPa to investigate the effect of confining pressure on stress–strain behavior. As confining pressure was elevated, the strength increased and material response changed from brittle fracture to ductile, strain-hardening behavior. Strain rate effect was investigated at confining pressure of 25 and 50 MPa for strain rates between 10^{-4} and 20/s. Ultimate strength and Young's modulus were observed to increase with increasing strain rate. Dry densities and porosities for selected samples were also measured.

TABLE OF CONTENTS

		Page
ABSTRACT		ii
LIST OF FIGURES		iv
LIST OF TABLES		v
ACKNOWLEDGMENTS		vi
1. INTRODUCTION		1
2. SITE DESCRIPTION		2
3. EXPERIMENTAL METHOD		6
4. RESULTS		7
4.1	Density and Porosity	7
4.2	Pressure-Volume Tests	10
4.3	Uniaxial Compression	11
4.4	Triaxial Compression	14
4.5	Intermediate Rate Tests	19
5. SUMMARY AND CONCLUSIONS		21
6. REFERENCES		22
APPENDIX 1. Description of Experimental Methods and Apparatus		23

LIST OF FIGURES

		Page
1.	Site topography and drill hole locations at PSA Flight 1771 crash site	3
2.	Geologic cross section A-A'	4
3.	Geologic cross section B-B'	5
4.	Outcrop material and associated samples	6
5.	Frequency distribution of sample density	9
6.	Relation of sample porosity to density	9
7a.	Pressure-volume behavior for material from drill core and outcrop sample	10
7b.	Pressure-volume behavior for outcrop samples	11
8.	Stress-strain behavior for samples loaded in uniaxial compression	13
9.	Relation of uniaxial compressive strength to sample density	13
10.	Uniaxial stress-strain behavior of outcrop material in directions parallel and perpendicular to bedding planes	14
11.	Stress-strain behavior for samples of drill core material tested at elevated confining pressure and strain rate of 10^{-4} s^{-1}	16
12.	Stress-strain behavior for drill core and outcrop samples tested at 50 MPa	17
13.	Stress-strain behavior for drill core and outcrop samples tested at 100 MPa	18
14.	Stress-strain behavior for drill core and outcrop samples tested at 250 MPa	18
15.	Axial and radial strain for sample tested at 25 MPa confining pressure	19
16.	Stress-strain behavior of samples tested at strain rates of 0.5 and 20 s^{-1} and confining pressure of 50 MPa	20
17.	Stress-strain behavior of samples tested at a strain rate of 20 s^{-1} and confining pressures of 25 and 50 MPa	20
A1.	Schematic of sample assembly for pressure-volume and confined compression tests	26
A2.	Schematic of system used for pressure-volume and confined compression tests at strain rate of 10^{-4} s^{-1}	27
A3.	Reaction frame used for pressure-volume and confined compression tests at strain rate of 10^{-4} s^{-1}	28
A4.	Cantilever system used to monitor radial deformation	29
A5.	Schematic of test system for uniaxial tests	30

LIST OF FIGURES
(continued)

		Page
A6.	Apparatus used for uniaxial tests	31
A7.	Schematic of system used for intermediate rate tests	32
A8.	Pictorial view of intermediate rate apparatus	33
A9.	Schematic of multipurpose digital data acquisition system	34
A10.	Multipurpose digital data acquisition system	35

LIST OF TABLES

		Page
1.	Summary data for laboratory tests	8
2.	Summary of uniaxial tests	12
3.	Summary of triaxial tests	15

ACKNOWLEDGMENTS

The work described in this report was carried out in support of the Plutonium Air Transport Certification (PATC) Project, which is currently being conducted by the Nuclear Systems Safety Program (NSSP) at Lawrence Livermore National Laboratory for the U.S. Nuclear Regulatory Commission (NRC). The work was funded by the Transportation Branch within the NRC's Office of Nuclear Materials Safety and Safeguards. John Cook was the NRC project monitor.

Garry Holman and Carl Walter of NSSP provided valuable technical and administrative reviews of this report, and C. K. Chou gave administrative guidance and support. Gerald Goudreau, Monika Witte, and Jim VanSant provided technical guidance in selection of appropriate testing parameters; David Carpenter and Mark Eli supplied the rock samples and sample descriptions. Carl Boro, Kirk Keller, and Robert Gibson assisted in fabrication and setup of test apparatus. Finally, Tonya Fletcher typed the manuscript and Lisa Hensel provided publication services.

1. INTRODUCTION

This report presents results of a laboratory testing program to determine mechanical properties of geologic materials from the PSA Flight 1771 crash site. The work was conducted in support of the Plutonium Air Transport Certification (PATC) Program and the Nuclear Systems Safety Program at Lawrence Livermore National Laboratory (LLNL). The objective of the testing was to provide information on the mechanical behavior of the rock at the PSA crash site at pressures in the range 0.1 to 500 MPa that are expected in a severe aircraft impact event. These constitutive relations will be used in modeling the impact surface for analyses of aircraft crashes in support of appropriate development tests for plutonium air transport (PAT) package designs. The mechanical behavior of the rock at the PSA crash site must be known to develop impact area requirements for a possible future aircraft crash test as severe as the PSA Flight 1771 accident.

A variety of laboratory tests and measurements were performed on samples derived from lengths of drill core and pieces of outcrop and float (surface-borne) material. Compressive strengths of most samples were tested at the strain rate of 10^{-4} s^{-1}. However, triaxial tests were also conducted at two intermediate strain rates (0.5 s^{-1} and 20 s^{-1}) for confining pressures of 25 and 50 MPa to determine the rate dependence of compressive behavior. Results reported here include pressure-volume (PV) behavior and bulk modulus to pressures of 500 MPa (72,500 psi), stress-strain behavior as a function of elevated pressure and strain rate, uniaxial strength, Poisson's ratio, and density/porosity relations. Material collected by drilling ranged from very friable and highly weathered material, which was unusable, to moderately dense, well-cemented sandstone. Work reported here focuses on weathered drill-core and outcrop and float samples.

Section 2 briefly describes the site and site geology. Section 3 presents an overview of experimental methods. Results are shown in Section 4 and a summary discussion is given in Section 5. The Appendix presents details of the experimental methods used in the testing.

2. SITE DESCRIPTION

All samples were from the PSA 1771 crash site near Paso Robles, California. This site is near the top of a steep east-facing hillside (see Fig. 1). The crash site is underlain by a sequence of interbedded clay shales and fine-grained sandstones mapped by Hall (see Ref. 1) as the late Mesozoic Toro Formation. Lenses of very hard calcareous siltstone and sandstone occur locally within these rocks. Beds within the shale-sandstone sequence are typically 6-75 mm thick. In the vicinity of the crash site, the beds strike northwest and dip 50-70 degrees toward the southwest. However, as a result of past tectonic activity, the beds of the Toro Formation at the crash site have been intensely fractured and sheared. In addition to this intense deformation, near-surface portions of the bedrock sequence have been further weakened by intense weathering and in-place decomposition. These processes have reduced the upper 4.5-9 m of the shale-sandstone sequence to materials in which the bedrock structure is generally visible but which have the geotechnical properties of hard soil or very weak rock A detailed description of the site can be found in Ref. 2.

Five core holes were drilled at this site (see Figs. 2 and 3), and specimens for laboratory testing were selected from the cores. Specimens of outcrop and float material were also collected during excavation associated with the dynamic penetrator testing (see Ref. 2 and Fig. 1 for location of penetrator tests). Samples prepared from this material will be referred to as outcrop samples in the remainder of this report. Much of the drill core and outcrop material was highly fractured and friable (RQD ≈ 30), and preparation of samples appropriate for testing at elevated pressures required great care. A typical piece of outcrop material and associated test samples are shown in Fig. 4.

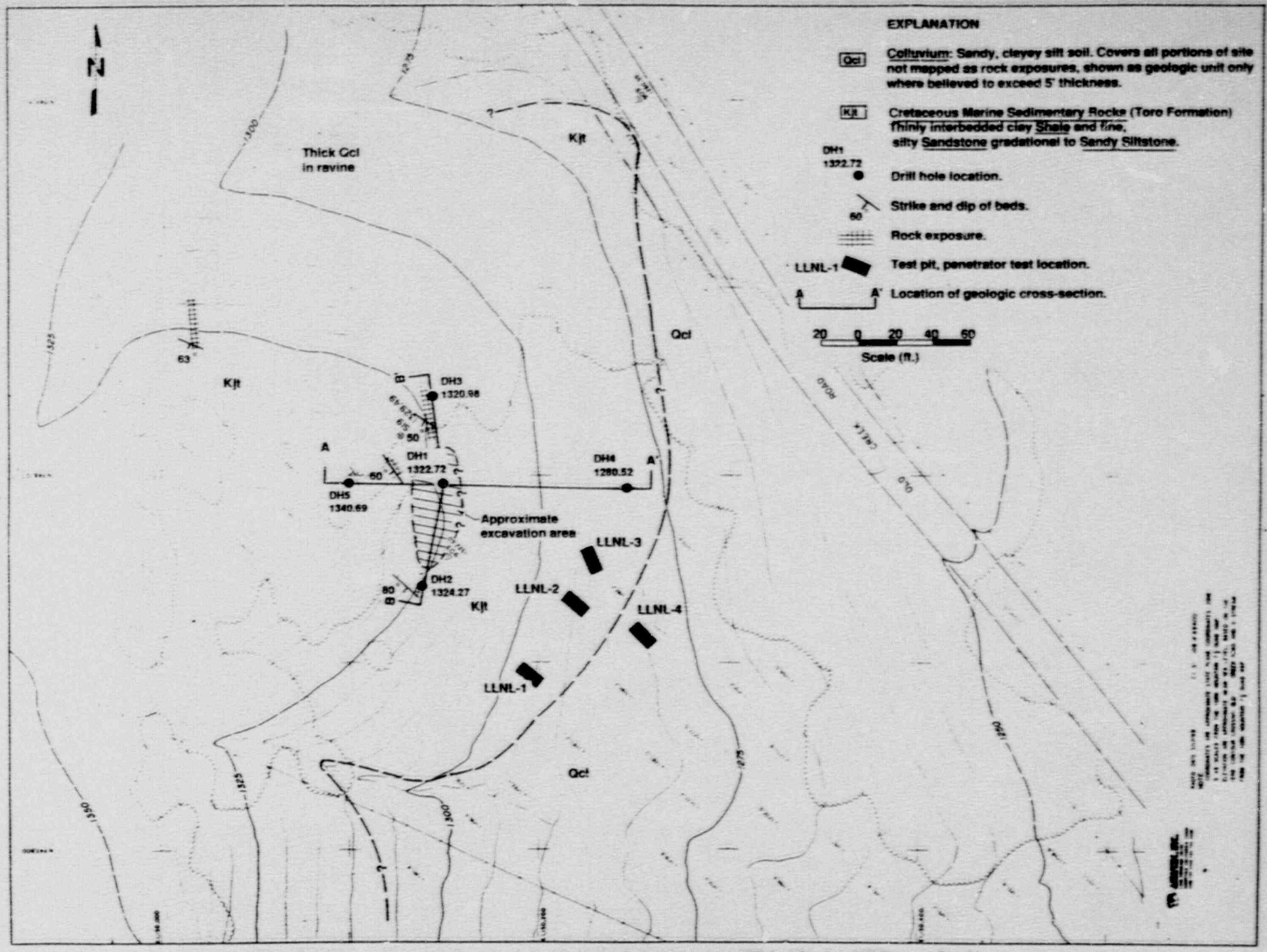

Fig. 1. Site topography and drill hole locations at PSA Flight 1771 crash site.

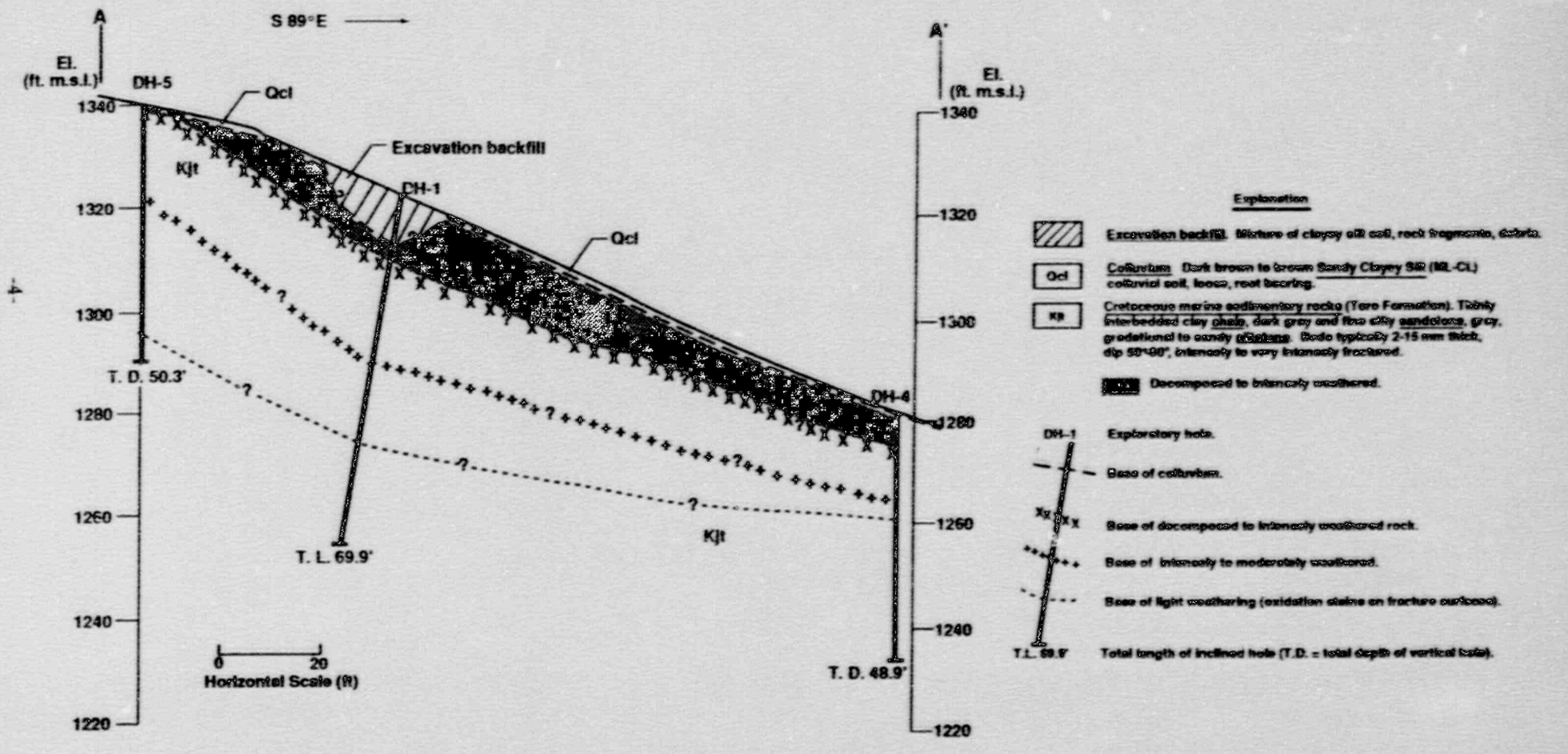

Fig. 2. Geologic cross section A-A'.

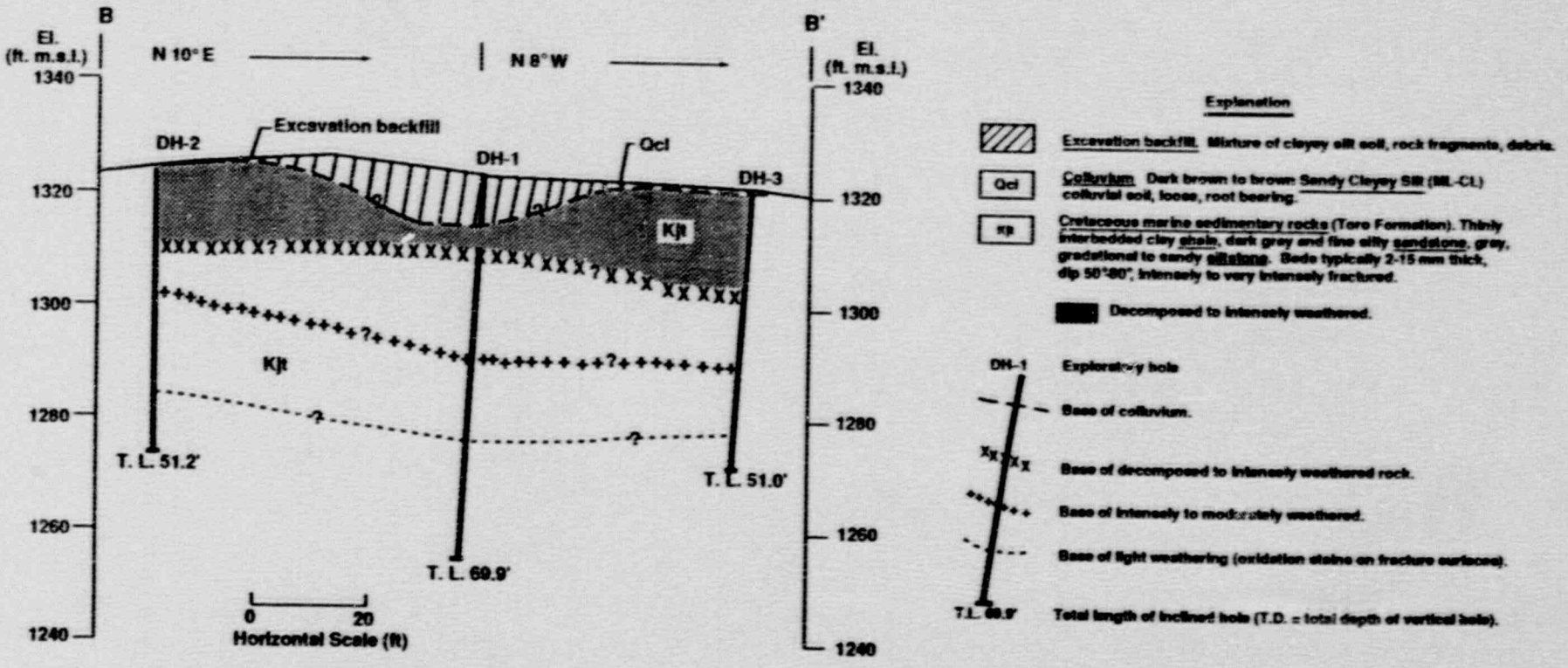

Fig. 3. Geologic cross section B-B'.

Fig. 4. Outcrop material and associated samples.

3. EXPERIMENTAL METHOD

Test samples were subcored from pieces of drill core and outcrop material and were prepared as right circular cylinders with diameter of 1 or 2 inches (2.54 or 5.08 cm) and length equal to twice the diameter. (Hereafter, for convenience and in order to use metric units, we will give these dimensions in centimeters, rounded off to 2.5, 5.1, and 10.2.) Tests were conducted in the rock mechanics laboratory at LLNL. Dry density was determined for all samples, and they all were tested dry. Porosity was determined for several samples using the wet/dry method. Samples tested in uniaxial compression were placed between two flat parallel platens in a stiff loading frame, and axial force was increased until failure occurred. Axial force was measured using a calibrated force gauge placed in series with the sample, and axial displacement was measured using a linear displacement transducer. Samples tested at elevated confining pressures were first placed between end caps and the jacketed with Viton (fluorel rubber) heat-shrink tubing to exclude confining fluid from the pore space of the sample. Pressure-volume tests were conducted by placing the sample assembly in a pressure vessel and then recording axial and radial deformation as a function of confining pressure. Radial deformation was measured inside the pressure vessel using a system of four strain-gauged cantilevers positioned against the central diameter of the sample. Axial displacement was measured outside the pressure vessel using a linear displacement transducer positioned to monitor displacement of the loading piston. For triaxial tests, at a strain rate of 10^{-4} s^{-1}, confining pressure was raised to the desired level and held constant while axial loading was applied. For these tests, radial and axial deformation were measured in the same way as for the pressure-volume tests. Axial force was measured with an internal force gauge placed in series with the sample. Triaxial tests at strain rates of 0.5 and 20 s^{-1} were conducted in an intermediate-strain-rate apparatus. This apparatus uses energy stored in a spinning flywheel to drive a piston that imposes axial stress on the sample. Radial strain was not measured in these tests, and axial deformation was calculated from flywheel speed. Details of the test apparatus and test procedures are given in the Appendix.

4. RESULTS

Tests conducted for this study are summarized in Table 1. For each sample, the table lists the type of test, core depth confining pressure, strain rate, and sample density. For drill core material the sample ID scheme follows the sample designations used by Carpenter, e.g. (see Ref. 2), DH1-4A and DH1-4B refer to two samples (A and B) prepared from piece 4 taken from drill hole DH1. Sample designations for outcrop material are prefixed with "OC". The outcrop sample designated OC1-1AP, for example, is the first sample (A) from "outcrop 1-1", with the P indicating that the core axis is parallel to the bedding planes. Similarly, outcrop sample OC1-1CV is the third sample (C) from "outcrop 1-1", with the V (for vertical) indicating that the core axis is perpendicular to the bedding planes. Results for particular tests are highlighted in the following sections.

4.1 Density and Porosity

Dry densities of the samples ranged from 2.15 g/cm^3 for weathered core and outcrop samples to 2.63 g/cm^3 for very competent, unweathered core samples. Sample density is given in Table 1, and a frequency plot of these densities is shown in Fig. 5. Density for weathered drill-core and outcrop samples was 2.15-2.45 g/cm^3. Unweathered drill-core samples had densities of 2.45-2.63 g/cm^3. Outcrop samples were slightly more dense than the weathered drill-core samples. Average density of outcrop samples was 2.31 g/cm^3.

Porosity was also determined for a few samples of drill core material, and a plot of porosity versus density is shown in Fig. 6. Porosity values are given in Table 1. These data fit the linear equation:

$$\phi = 1.0 - 0.372\,\rho,$$

where:

ϕ = porosity,

ρ = density (g/cm^3).

Table 1. Summary data for laboratory tests.

Sample ID	Core Depth (ft)	Density (g/cm^3)	Porosity	Confining Stress (MPa)	Strain Rate (s^{-1})
DH1-3	11.6	2.15	---	---	---
DH1-4A	14	2.27	---	500	10^{-4}
DH1-4B	14	2.20	---	25	10^{-4}
DH1-5	27	2.22	---	50	10^{-4}
DH2-3A	11.5	2.25	---	250	10^{-4}
DH2-3B	11.4	2.19	---	500	10^{-4}
DH2-4A	20.1	2.28	---	---	---
DH2-4B	20.1	2.36	---	---	---
DH2-4C	20.1	2.23	0.25	---	---
DH2-6A	31.3	2.42	---	---	---
DH2-7B	36.5	2.63	---	---	---
DH2-7C	36.5	2.62	---	0.1	10^{-4}
DH2-8A	44.4	2.49	---	0.1	10^{-4}
DH3-5	20.4	2.37	---	500	10^{-4}
DH3-6AV	23	2.22	---	50	0.5
DH3-6B	23	2.24	---	25	0.5
DH4-4	21.3	2.59	---	0.1	10^{-4}
DH4-5	26.4	2.53	---	0.1	10^{-4}
DH4-6A	38.3	2.49	0.06	---	---
DH4-6B	38.3	2.52	0.05	---	---
DH4-7	46.4	2.42	---	0.1	10^{-4}
DH5-3A	5.7	2.21	---	100	10^{-4}
DH5-3B	5.7	2.22	0.16	---	---
DH5-4A	13.6	2.29	---	0.1	10^{-4}
DH5-7B	28	2.61	0.01	---	---
DH5-8A	34.7	2.40	---	---	---
DH5-8B	34.7	2.42	0.11	---	---
OC1-1AP	---	2.21	---	50	0.5
OC1-1BP	---	2.23	---	50	0.5
OC1-1CV	---	2.24	---	50	0.5
OC1-V	---	2.22	---	500	10^{-4}
OC2-AP	---	2.28	---	---	10^{-4}
OC2-BP	---	2.29	---	---	---
OC2-CP	---	2.31	---	50	10^{-4}
OC2-AV	---	2.34	---	100	10^{-4}
OC2-BV	---	2.34	---	250	10^{-4}
OC2-4AP	---	2.30	---	0.1	10^{-4}
OC2-4BP	---	2.32	---	0.1	10^{-4}
OC2-4CP	---	2.39	---	---	---
OC2-4DP	---	2.33	---	---	---
OC2-4AV	---	2.38	---	0.1	10^{-4}
OC2-4BV	---	2.34	---	0.1	10^{-4}
OC2-4CV	---	2.38	---	---	---
OC2-4DV	---	2.36	---	---	---
OC2-4EV	---	2.37	---	---	---
OC3-AV	---	2.31	---	25	20
OC3-BV	---	2.28	---	50	20

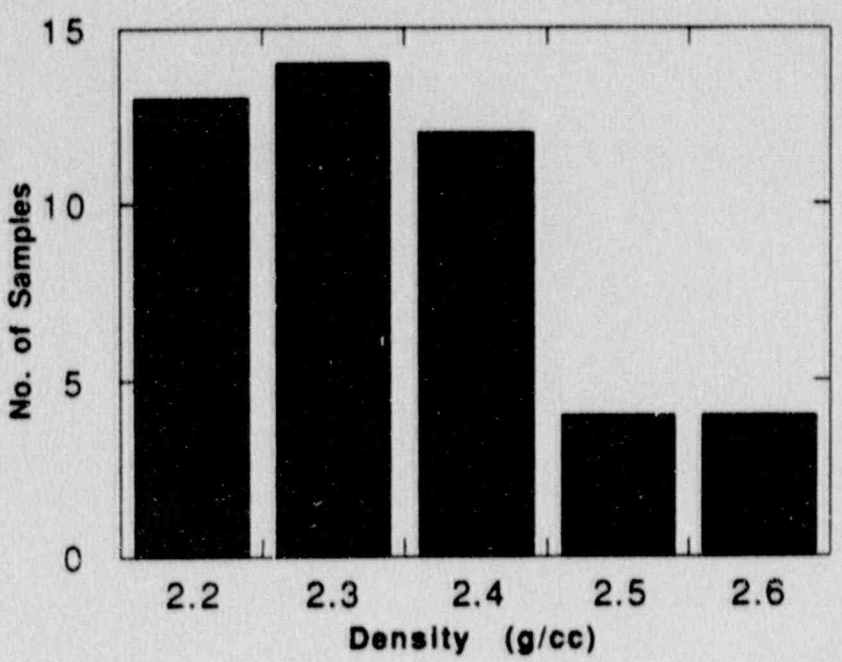

Fig. 5. Frequency distribution of sample density.

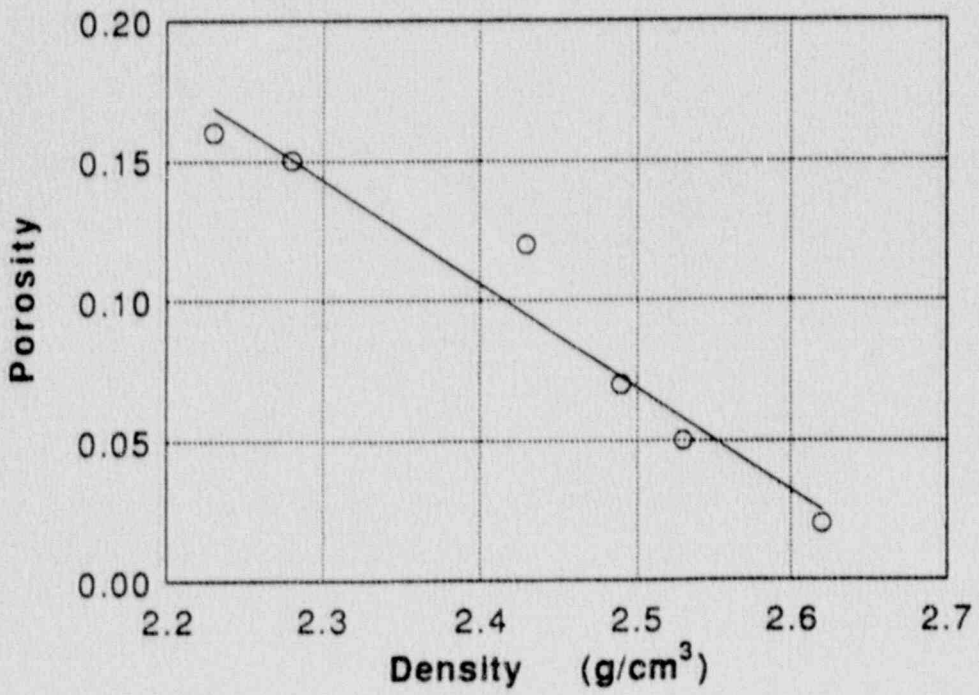

Fig. 6. Relation of sample porosity to density.

4.2 Pressure-Volume Tests

Pressure-volume tests were conducted on samples of drill core and outcrop material. Tests to confining pressures of 480 and 400 MPa were conducted on samples of diameter 2.5 cm and length 5.1 cm. The pressure-volume curves for these samples are shown in Fig. 7a. Both are concave upward, as is common for rocks. The curve for the drill core sample has two distinct regions. The behavior in the first region (0–70 MPa) is controlled by closure of preexisting fissures and large voids; the minerals are slightly compressed in this region. In the second region, above 70 MPa, the deformation is controlled by deformation of pores and compression of grains; the rock behaves linearly in this region (see Ref. 3). Bulk modulus determined from unloading for this second region is 6.58 GPa for the drill core sample. The outcrop material was cored perpendicular to the bedding planes found in the specimen. It can be seen that, at pressures below 200 MPa, this sample was much less compressible than was the drill core sample. However, at pressures above 200 MPa, the behavior of both samples is very similar. Bulk modulus determined for the outcrop sample is 6.25 GPa. Fig. 7a shows that bulk modulus is very similar for the two samples once fractures and voids are closed.

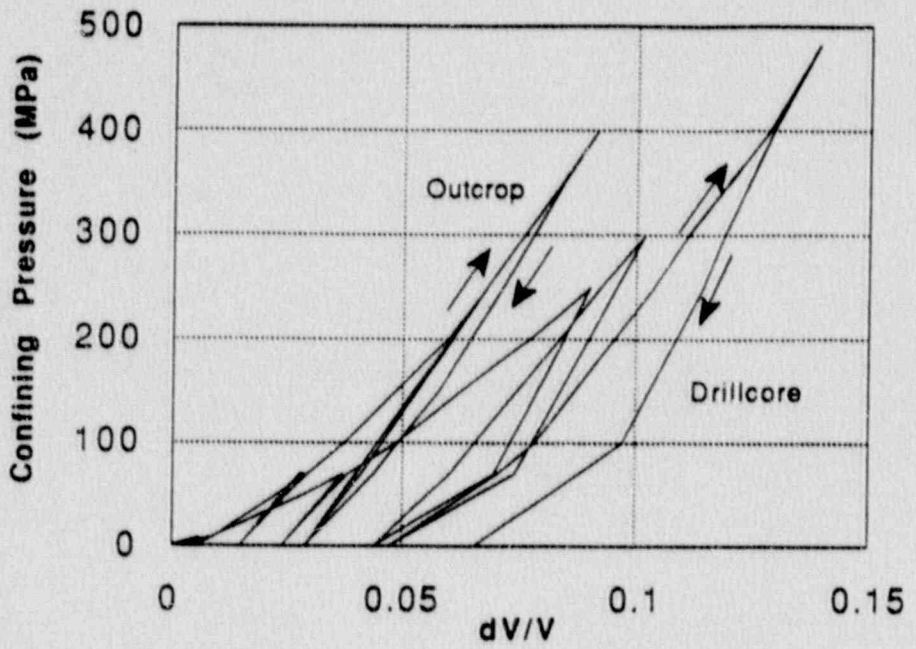

Fig. 7a. Pressure-volume behavior for material from drill core and outcrop samples.

Pressure-volume tests were also conducted on two larger samples of outcrop material. These samples were 5.1 cm in diameter by 10.2 cm long and were tested to pressures of 150 and 100 MPa, respectively. Results from these two samples were very similar, and data for one of them are shown in Fig. 7b along with the pressure-volume response of the 2.5-cm-diameter outcrop sample. This figure shows that sample size had very little effect on pressure-volume behavior in the pressure range 0-70 MPa.

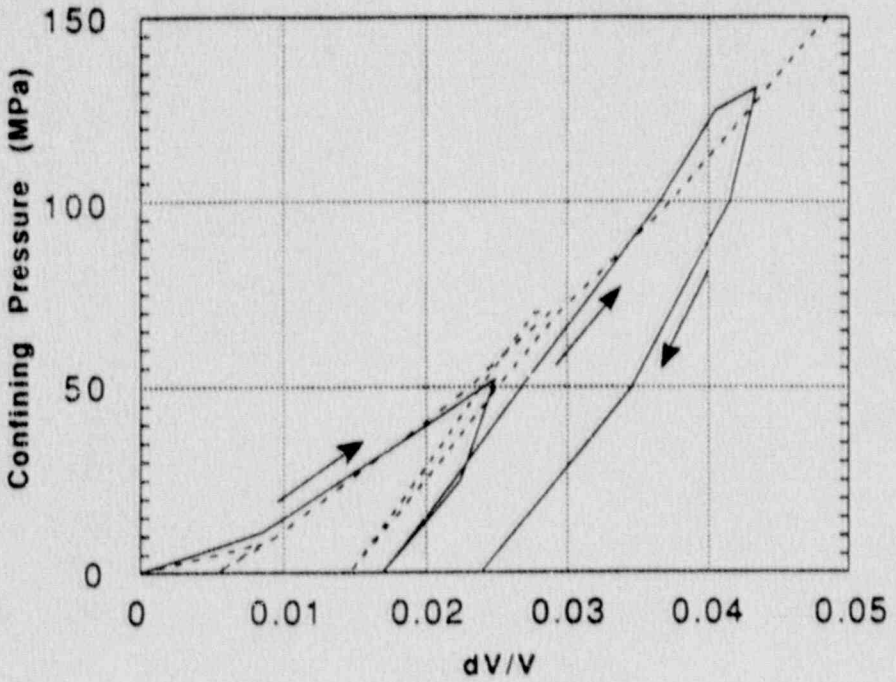

Fig. 7b. Pressure-volume behavior for outcrop samples.

4.3 Uniaxial Compression

Uniaxial compression tests were conducted on several samples of drill core and outcrop material to determine uniaxial strength and Young's modulus for these materials. Results are summarized in Table 2. Stress-strain curves for selected samples are plotted in Fig. 8, along with a representative curve for concrete. This figure shows that one sample (DH2-7C) had uniaxial strength of more than 130 MPa and Young's modulus similar to that of concrete. This sample consisted of unweathered sandstone with calcite cement. Samples prepared from weathered drill core and outcrop materials were much weaker, with uniaxial strength of 17-30 MPa and Young's modulus of 1.3-3.5 GPa. These were samples with lower density. Samples often broke along shale interbeds. A plot of uniaxial strength as a function of sample density is shown in Fig. 9. This plot shows that, for most samples, uniaxial strength was proportional to the sample density and was independent of sample diameter. This proportionality can be described by the equation:

$$S = -718 + 317\,\rho,$$

where:

S = uniaxial strength (MPa),

ρ = density (g/cm^3).

Uniaxial strength versus sample orientation with respect to bedding planes was also investigated for outcrop materials. Two test specimens were taken in directions parallel and perpendicular to the bedding present in the outcrop material. These specimens were 5.1 cm in diameter by 10.2 cm long. Uniaxial stress-strain curves for these four samples are shown in Fig. 10. These data indicate that the outcrop material is somewhat stronger and has a higher Young's modulus in the direction perpendicular to the bedding planes.

Table 2. Summary of uniaxial tests.

Sample	Ultimate Strength (MPa)	Young's Modulus (GPa)	Sample Diameter (cm)
	Drill Core Samples		
DH2-7C	133	14.67	2.5
DH2-8A	17*	2.90	2.5
DH4-4	88	9.81	2.5
DH4-5	143	11.92	2.5
DH4-7	42	---	2.5
DH5-4A	22	1.88	2.5
	Outcrop Samples		
OC2-4AP	8	2.60	5.1
OC2-4AV	30	5.60	5.1
OC2-4BP	21	3.30	5.1
OC2-4BV	23	3.80	5.1

* Sample failed along bedding plane.

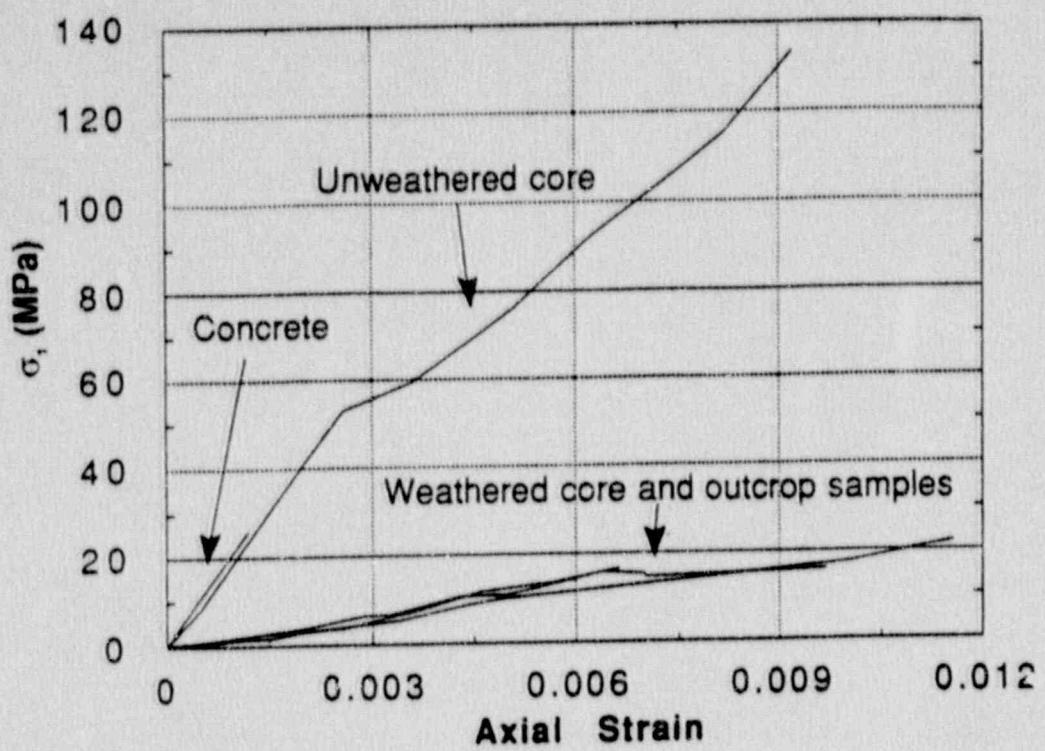

Fig. 8. Stress-strain behavior for samples loaded in uniaxial compression.

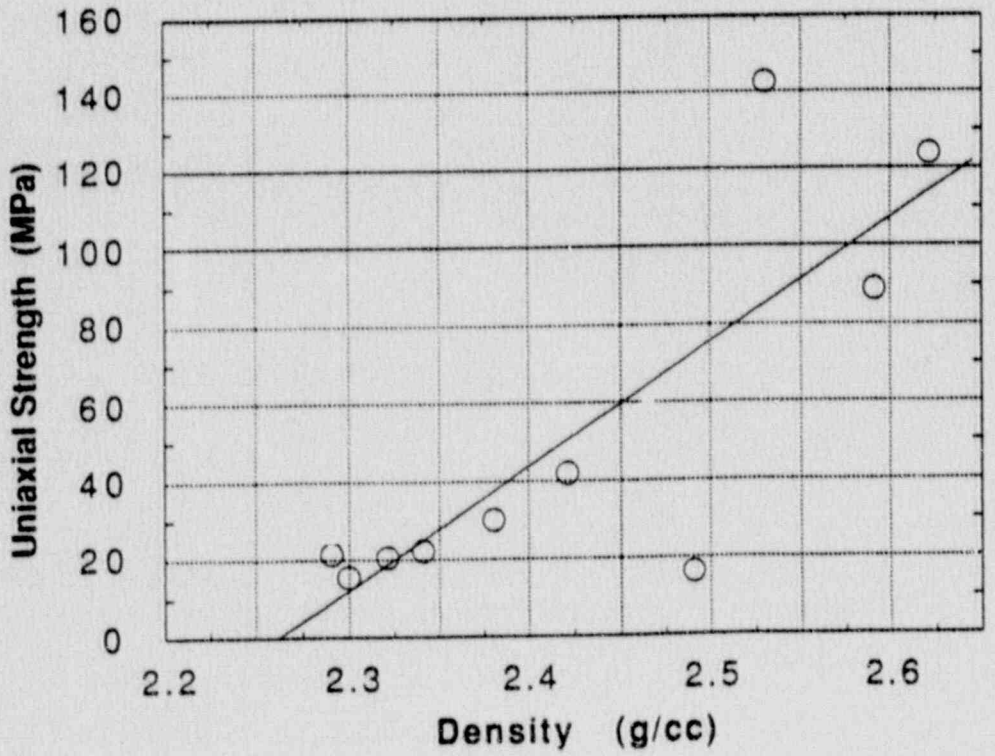

Fig. 9. Relation of uniaxial compressive strength to sample density.

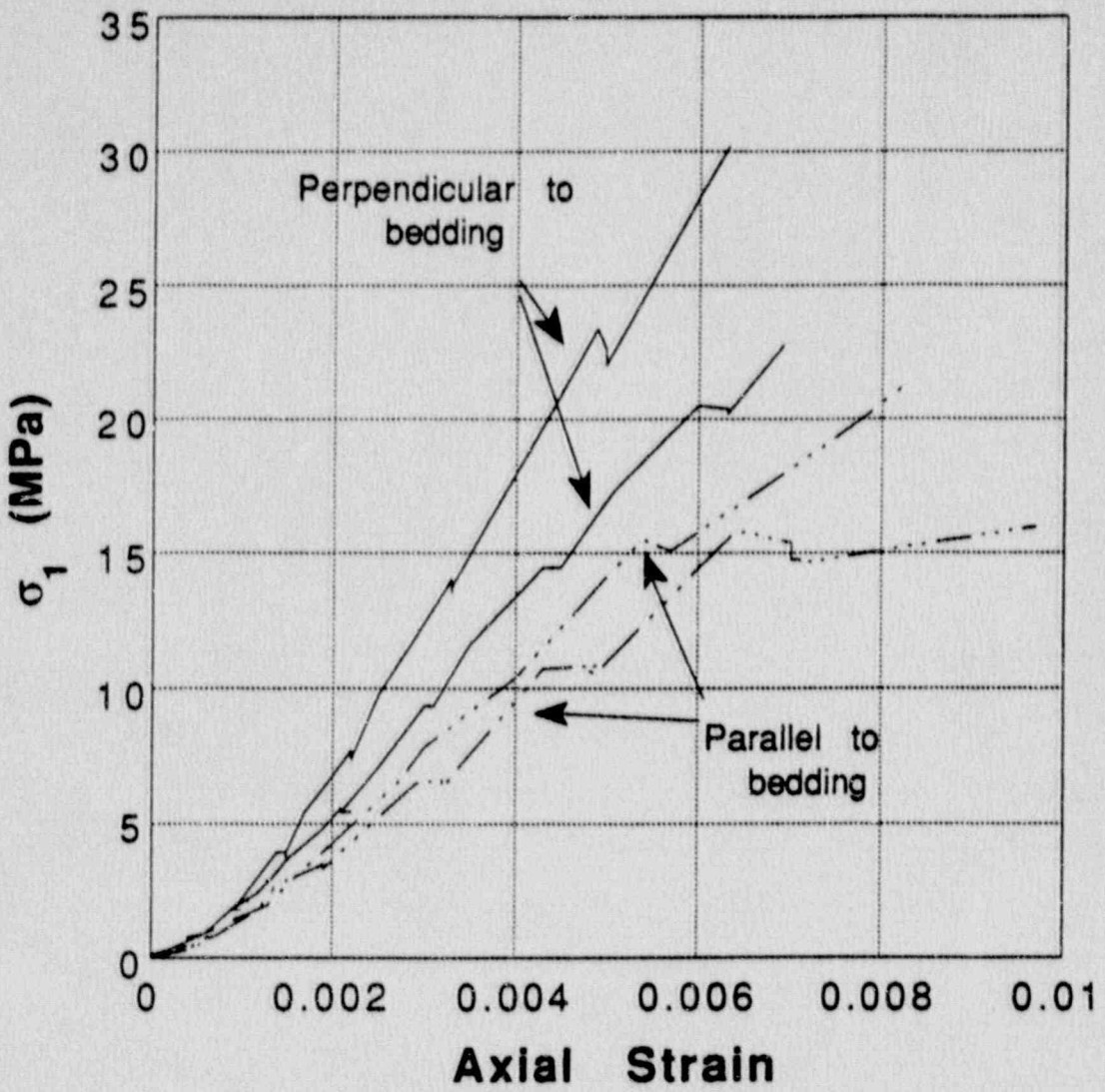

Fig. 10. Stress–strain behavior of outcrop samples cored parallel and perpendicular to bedding planes in uniaxial compression.

4.4 Triaxial Compression

Several samples of drill core and outcrop material were tested in triaxial compression at three different strain rates to determine the effect of confining pressure and strain rate on stress-strain behavior. All triaxial tests were conducted on samples with diameter of 2.5 cm. Results are summarized in Table 3. Stress-strain curves for samples of drill core tested at pressures between 25 and 500 MPa at a strain rate of 10^{-4} s^{-1} are shown in Fig. 11. This figure shows that the samples tested at 25 and 50 MPa behaved in a semibrittle manner, while samples tested at pressures

of 100 MPa and above displayed ductile, strain-hardening behavior, with compressive strength increasing with strain at higher confining pressures. This may be due to pore crush-up, which occurs at elevated pressures and stresses when the cementing material between grains yields and pore space is reduced as the grains become more tightly packed. Petrographic study of tested samples would be required to confirm this hypothesis.

Table 3. Summary of triaxial tests.

Sample	Strain Rate (s^{-1})	Confining Pressure ($\sigma_2 = \sigma_3$) (MPa)	Ultimate Strength ($\sigma_1 - \sigma_3$) (MPa)	Young's Modulus[a] (GPa)
		Drill Core Samples		
DH1-4B	0.0001	25	175	4.86
DH1-5	0.0001	50	180	4.25
DH5-3A	0.0001	100	160[b]	4.32
DH2-3A	0.0001	250	220[b]	6.43
DH1-4A	0.0001	500	360[b]	7.40
		Outcrop Samples		
OC2-CP	0.0001	50	182	5.00
OC2-AV	0.0001	100	260	7.00
OC2-BV	0.0001	250	340	7.83
DH3-6B	0.5	25	139[c]	---
DH3-6AV	0.5	50	179	---
OC1-1CV	0.5	50	175	4.03
OC3-AV	20	25	188	6.25
OC3-BV	20	50	212	6.23

[a] Young's modulus determined at axial strain = 0.03.

[b] $\sigma_1 - \sigma_3$ at 5% axial strain.

[c] Sample failed along preexisting fracture.

All tests on 2.5-cm-diameter samples.

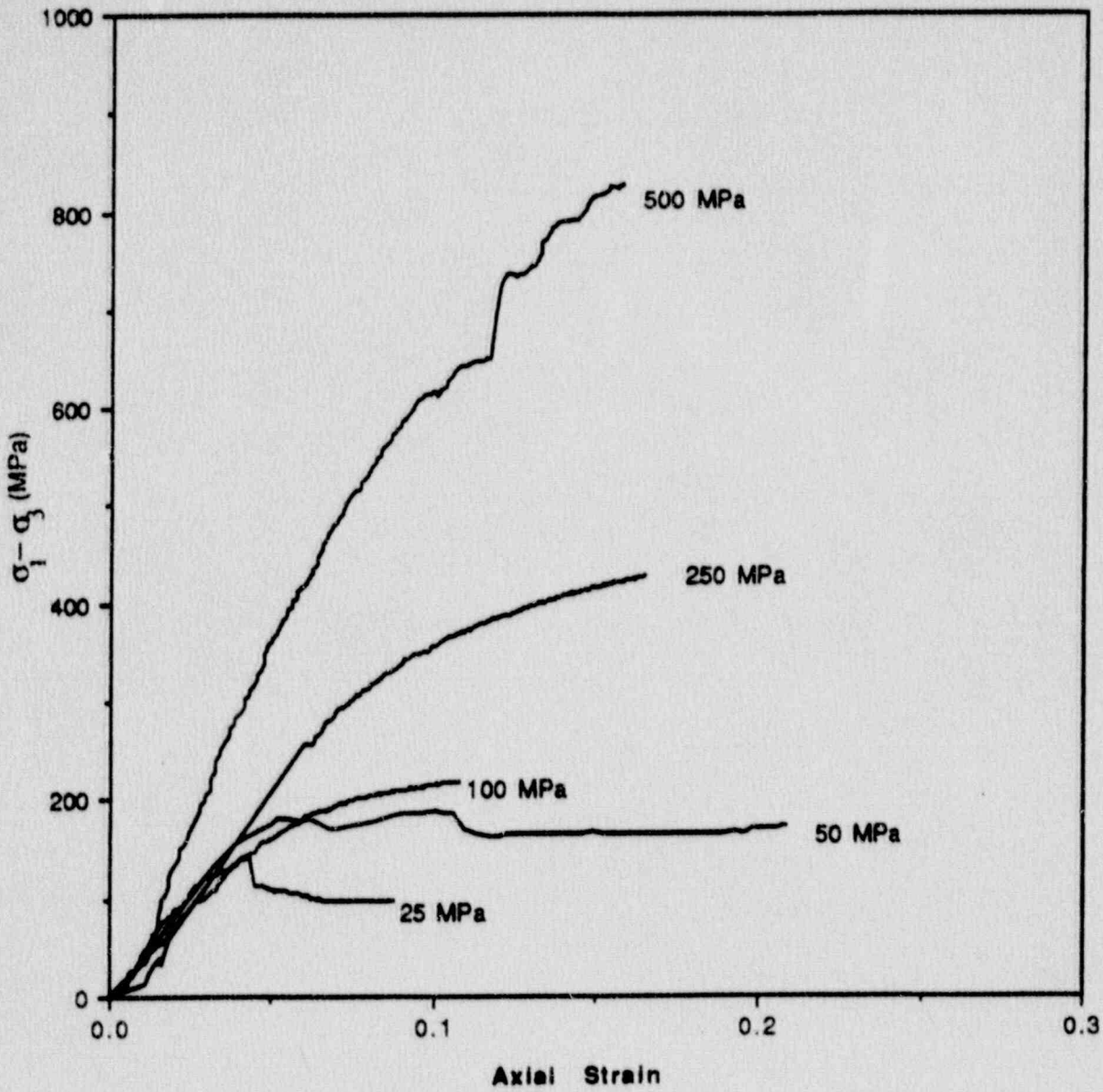

Fig. 11. Stress-strain behavior for samples of drill core material tested at elevated confining pressure and strain rate of 10^{-4} s^{-1}.

A suite of triaxial tests was also conducted on samples from outcrop material. Stress-strain behavior of this material at confining pressures of 50, 100, and 250 MPa and a strain rate of 10^{-4}/s are plotted in Figs. 12, 13, and 14. For comparison, stress-strain data for the drill core samples tested at these conditions are also shown.

Figure 12 shows that, at a confining pressure of 50 MPa, both drill core and outcrop material exhibited semibrittle behavior, with similar values of peak and residual differential stress. Stress-strain behaviors for outcrop and drill core samples tested at 100 MPa confining pressure are shown in Fig. 13. The figure shows that these two samples behaved much differently at this confining pressure. The outcrop material behaves in a semibrittle manner, with a modulus of 7.8 GPa and differential stress that remains almost constant as axial strain is increased beyond 0.05. The drill core has a much lower modulus (3.4 GPa) and shows strain-hardening behavior throughout the axial deformation. Although the outcrop sample is stronger, values of differential stress for the two samples are similar at strains above 0.1.

Figure 14 shows stress-strain behavior for outcrop and drill-core samples tested at a confining pressure of 250 MPa. Behavior of the outcrop material is again semibrittle, with differential stress remaining constant at strains greater than 0.05. The drill core material again shows a lower modulus and strain-hardening behavior. The outcrop material is stronger at axial strains below 0.09; however, at strains greater than 0.09, the drill core material is stronger due to the continued strain-hardening behavior. Ultimate strength and Young's modulus values determined for these tests are tabulated in Table 3.

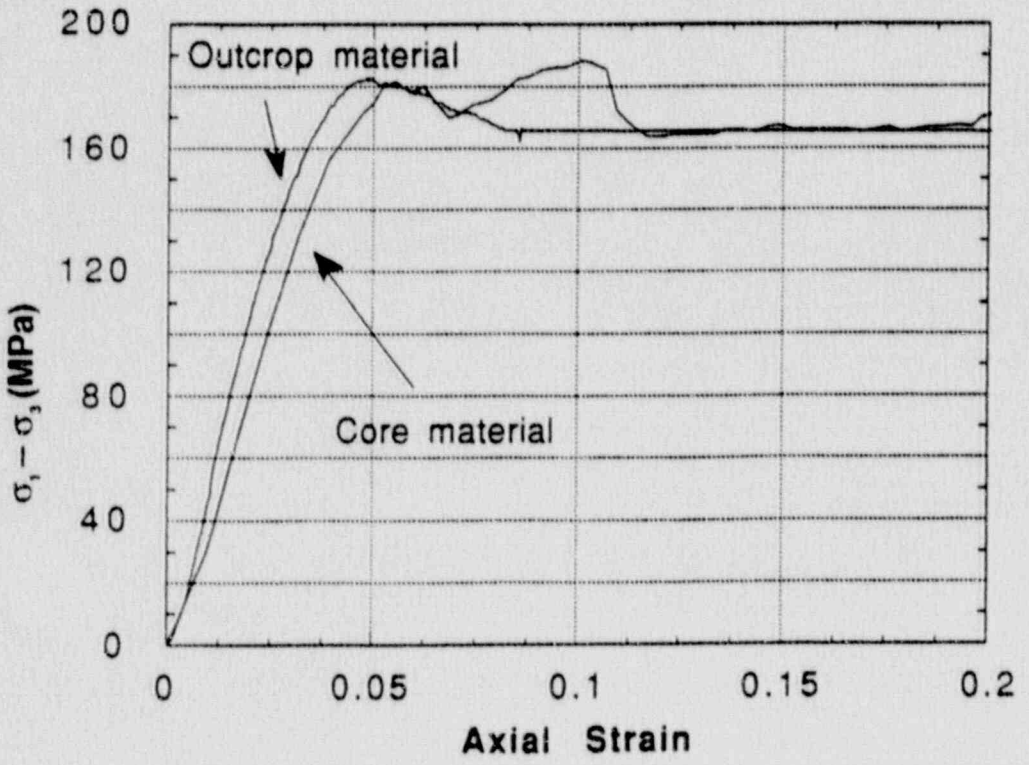

Fig. 12. Stress-strain behavior for drill core and outcrop samples tested at 50 MPa.

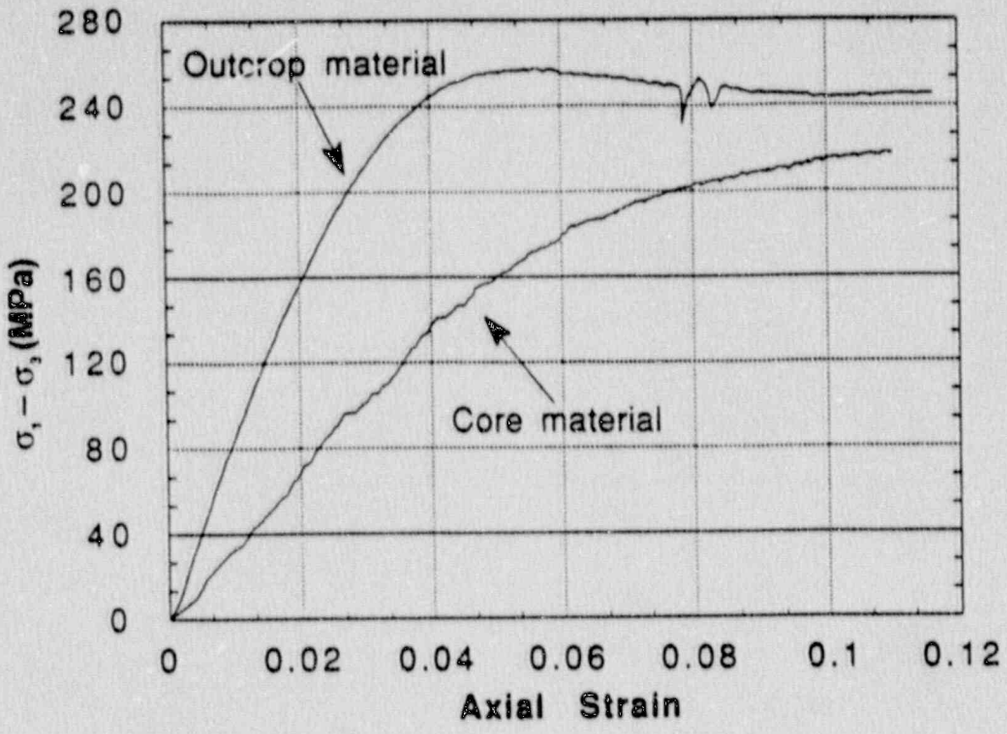

Fig. 13. Stress-strain behavior for drill core and outcrop samples tested at 100 MPa.

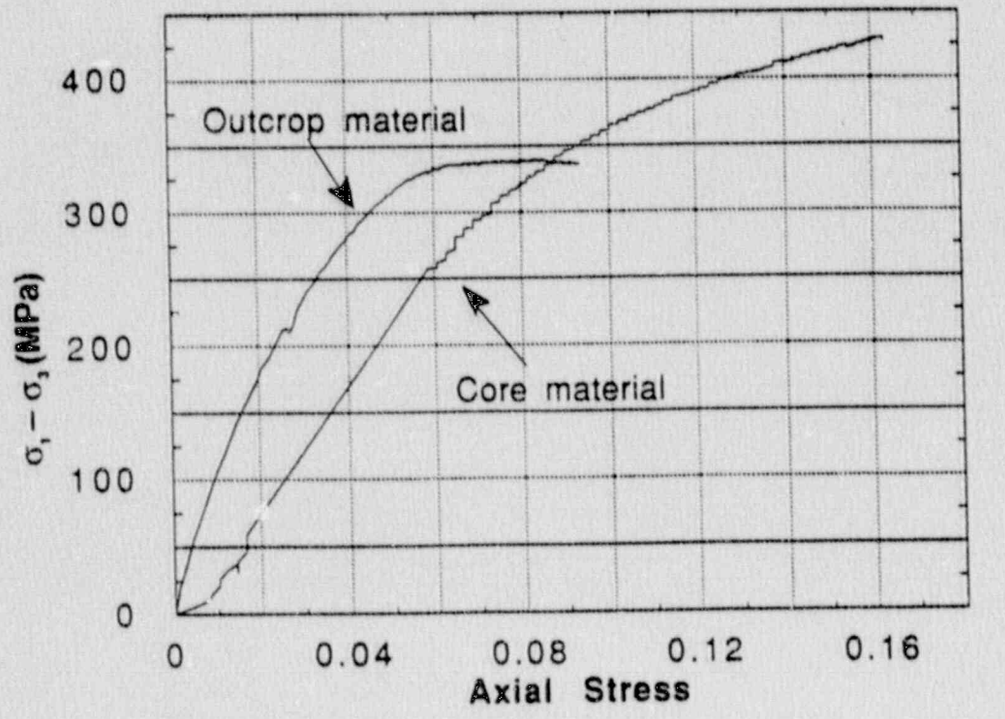

Fig. 14. Stress-strain behavior of drill core and outcrop samples tested at 250 MPa.

Poisson's ratio was determined for selected samples by dividing the radial strain by the axial strain. A typical plot of radial and axial strains for a sample tested at 25 MPa is shown in Fig. 15. Possion's ratio was found to be in the range 0.25-0.28. This agrees well with values calculated from acoustic velocity data collected at the site (see Ref. 4).

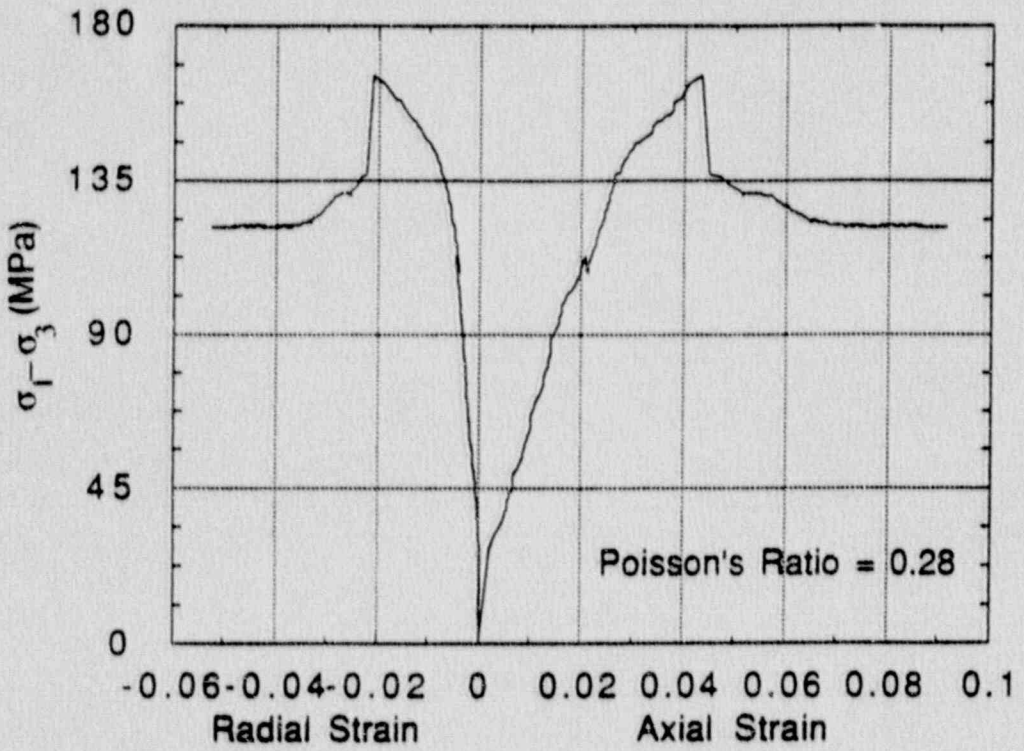

Fig. 15. Axial and radial strains for sample DH1-4B tested at 25-MPa confining pressure.

4.5 Intermediate Rate Tests

Triaxial tests were also conducted at two intermediate strain rates to determine the rate dependence of compressive behavior. Stress-strain curves for tests conducted at confining stress of 50 MPa and strain rates of approximately 0.5 and 20 s^{-1} are shown in Fig. 16.

Data for the test at 0.5 s^{-1} yield values of ultimate strength and Young's modulus similar to those determined during the slower tests. The values of ultimate strength and Young's modulus (Table 3) for the test at 20 s^{-1} are somewhat higher than those observed at the slower speeds.

Results of tests at 25 and 50 MPa at a strain rate of 20 s^{-1} are shown in Fig. 17. This figure shows that at axial strains less than about 0.035, the behavior of the two samples was very similar. However, the sample tested at 25 MPa shows semibrittle or transitional behavior, and planes of brittle fracture were evident in the sample. The sample tested at 50 MPa behaved in a more ductile manner. This is consistent with tests at the slower rates.

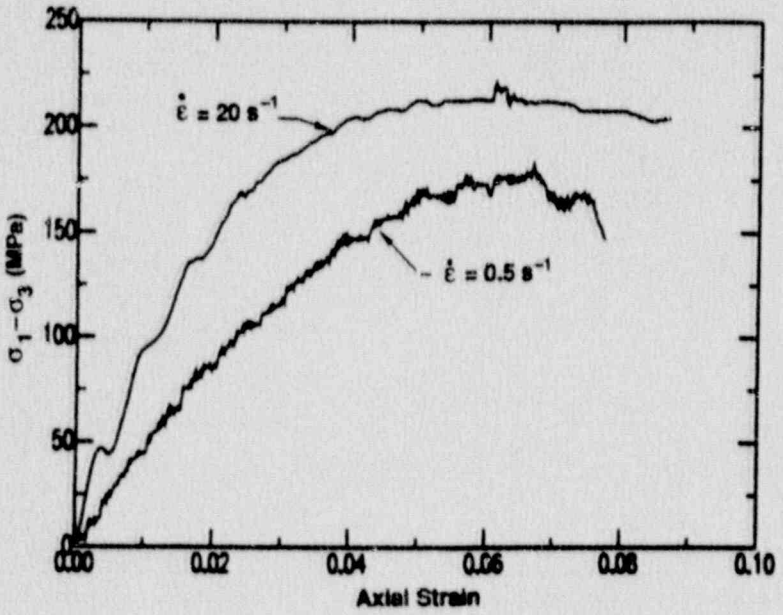

Fig. 16. Stress-strain behavior of samples tested at strain rates of 0.5 and 20 s^{-1} and confining pressure of 50 MPa.

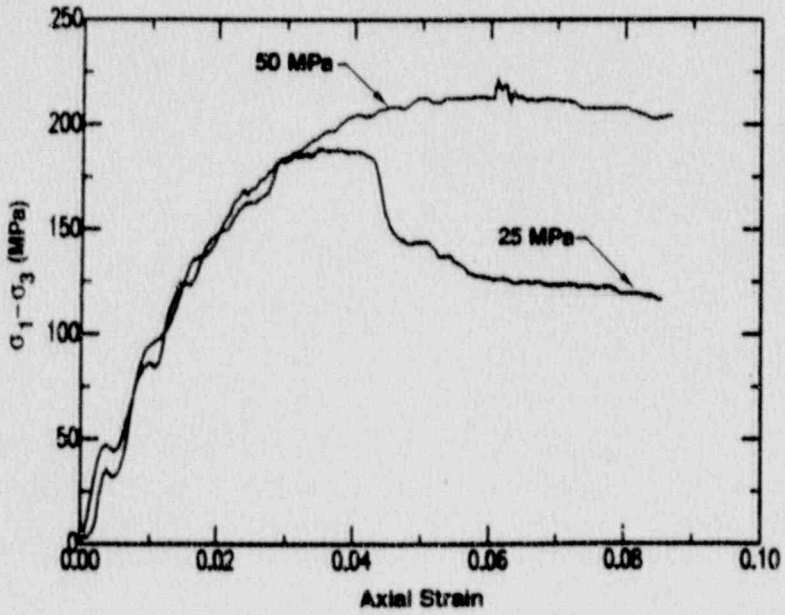

Fig. 17. Stress-strain behavior of samples tested at a strain rate of 20 s^{-1} and confining pressures of 25 and 50 MPa.

5. SUMMARY AND CONCLUSIONS

Results of tests and measurements reported here define several of the mechanical properties of the geologic materials at the PSA Flight 1771 crash site that are necessary to formulate a constitutive model for this site. Most of the samples chosen for testing were of weathered drill-core and outcrop material, although some samples of unweathered drill-core material were tested. The pressure-volume behavior and bulk modulus of the material are important inputs to the constitutive model, but we found the values of bulk modulus measured on laboratory test samples might lead to an overestimate of the stiffness of the site by a significant amount since these data represent behavior of small intact samples while, in fact, the rock at the site is highly fractured (see Refs. 2 and 5). It is important to note that measurement of bulk modulus to pressures above a few tens of MPa (a few thousand psi) on large samples is difficult due to the fractured and friable nature of the rock (we were unable to obtain core specimens larger than 5.1 cm in diameter) and the limitations of the experimental apparatus.

Uniaxial tests showed the material to be in the strength range of medium strength rock (see Ref. 6). Some anisotropy was observed in outcrop samples, as those taken perpendicular to the bedding had a higher uniaxial strength than those taken parallel to the bedding. Uniaxial strength was similar for both 2.5-cm-diameter and 5.1-cm-diameter samples. Moreover, uniaxial strength was well correlated with sample density.

Confined compressive tests showed that the brittle/ductile transition occurred at pressures in the range of 25-50 MPa. Samples prepared from drill core material showed strain-hardening behavior at confining pressures of 100 MPa and greater, and yield criteria are difficult to apply to these samples. The strain hardening may be caused by a mechanism of gradual pore crush-up, where the cementing and pore-filling agents between grains fail as axial load is applied. As the cement fails, porosity is reduced, more and more grains come into contact, and the material strength increases.

The outcrop material behaved very similarly to the drill-core material at confining pressures of 0.1 (unconfined) and 50 MPa. However, at higher confining pressures of 100 and 250 MPa, the outcrop material behaved in a semibrittle manner. Young's modulus also increased with increased confining pressure. This behavior may be due to the effect of near-surface weathering on the rock. However, detailed study of this behavior is beyond the scope of this report.

Results also show that raising the strain rate from 10^{-4} s^{-1} to 0.5 s^{-1} did not affect compressive behavior significantly. However, raising the strain rate to 20 s^{-1} caused an increase in ultimate strength and in Young's modulus for samples tested at confining pressures of 25 and 50 MPa.

6. REFERENCES

1. C. A. Hall, Geologic Map of Cambria Region, San Luis Obispo County, California, U.S.G.S. Miscellaneous Field Studies, Map MF-599 (1974).

2. D. W. Carpenter, J. C. Chen, and G. S. Holman, An Engineering Geologic Evaluation of the PSA Flight 1771 Cash Site Near Paso Robles, California, Lawrence Livermore National Laboratory, PATC-IR 89-04 (1989).

3. R. E. Goodman, Introduction to Rock Mechanics, Wiley & Sons, New York, 1980.

4. Endacott & Associates, Shear Wave Investigation PSA Crash Site, Paso Robles, California, report to LLNL (April 17, 1989).

5. F. E. Heuze, Scale Effects in the Determination of Rock Mass Strength and Deformability, *Rock Mechanics*, 12, pp. 167-192 (1980).

6. D. V. Deere and R. P. Millar, Engineering Classification and Index Properties for Intact Rock, Air Force Weapons Laboratory, Kirtland AFB, New Mexico, Technical Report AFWL-TR-65-116 (1966).

APPENDIX 1. Description of Experimental Methods and Apparatus.

A1. SAMPLE PREPARATION

Specimens for testing were prepared from core material recovered from drill holes at the field site and from samples collected from outcrops and trenches dug at the site. Test specimens 2.5 cm (1 in.) in diameter were subcored from the drill core and surface samples. Samples for compression and pressure-volume tests were trimmed to a length of 5.1 cm (2 in.). Test specimens with diameters of 5.1 cm and lengths of 10.2 cm (4 in.) were also produced from surface samples. Test specimens were prepared as right circular cylinders with ends ground flat and parallel within 0.025 mm. Some samples were quite fractured and friable. Small amounts of epoxy were used to hold chips in place or to fill small voids. All samples were dried in a vacuum oven at 30°C for several days prior to testing. Sample weight was checked periodically, and a sample was assumed dry when no measurable weight change occurred during a period of 24 hours. All samples were tested dry. Sample length, diameter, weight, and other data were recorded in laboratory notebooks and entered into a computerized data base for easy recall.

A2. DENSITY AND POROSITY

Dry bulk density was determined for all samples by simply dividing the dry weight by the sample volume. Dry weight was the weight of the sample after drying in a vacuum oven as described in Section A1. Porosity was determined for a number of samples using the wet/dry method. Samples were first vacuum-dried at about 30°C until constant weight was observed over a 24-hour period. The samples were then saturated with water using the following procedure: The samples were placed in a sealed chamber and the chamber was evacuated; the chamber was then filled with water and pressurized to approximately 0.69 MPa (100 psi) for several days. The samples were weighed periodically and were assumed to be saturated when no weight change occurred during a period of 24 hours. The volume of pore space was calculated based on weight of water absorbed into the sample (1 gram of water = 1 cm^3). Porosity was calculated as the volume of pores divided by the volume of the whole sample.

A3. MECHANICAL PROPERTIES

A3.1 Pressure-Volume Tests

Pressure-volume tests were conducted on two samples that were 2.5 cm in diameter by 5.1 cm long. Each sample was prepared for the test assembly by placing an end cap at each end and then jacketing the sample with Viton (fluorel rubber) heat-shrink tubing. Sample assemblies are shown in Fig. A1. Tests were conducted using the

system depicted in Fig. A2. Oil was used as a confining medium. The pressure vessel was placed in a load frame (Fig. A3) and connected to a pressurizing system. Confining pressure was imposed by increasing the pressure of the oil surrounding the sample. Confining pressure was monitored using a calibrated Heise gauge and the results were recorded in a laboratory notebook. Radial deformation at the horizontal midplane of the sample was monitored using a system of four cantilever arms shown in Fig. A4. Axial deformation was monitored at each pressure step by recording the position of the loading piston when it contacted the sample at that pressure. Contact of the loading piston with the sample was determined from response of both the cantilever system and the internal load cell. For the 5.1-cm-diameter samples, mechanical contact of the load ram was also determined electrically via contact of electrodes attached to the sample and the load ram. After each axial strain measurement, the loading piston was retracted from the sample to prevent axial deformation. Axial and radial deformation data were recorded using the multipurpose data acquisition system described in Section A4.

Cantilever data were corrected for pressure effects, then converted to radial strain. Uniform radial strain along the axis of the cylinder was assumed in the calculation of the change in volume.

A3.2 Uniaxial and Triaxial Tests

Series of compression tests were performed at three different strain rates. These tests provided data on the uniaxial strength, Young's modulus, shear modulus, Poisson's ratio, and Mohr-Coulomb failure envelope as a function of strain rate. In particular, samples were tested at strain rates of 10^{-4}, 0.5, and 20 s^{-1}.

A3.2.1 Low-Strain-Rate Tests

Uniaxial tests at this strain rate (10^{-4} s^{-1}) were conducted on unjacketed samples using the apparatus shown in Figs. A5 and A6. Displacement of the loading platen was monitored using a linear displacement transducer; axial load was measured using a load cell placed in series with the sample. Load and displacement data were recorded using the multipurpose data acquisition system described in Section A4.

Triaxial tests at a strain rate of 10^{-4} s^{-1} were conducted using the apparatus depicted in Figs. A2 through A4. Oil was used for the confining fluid in these tests. Samples were prepared as for the pressure-volume tests, with end caps and a fluorel rubber jacket (see Fig. A1). The sample was placed in the pressure vessel, and the vessel was assembled into the loading frame. Confining pressure was raised to the desired level by pressurizing the oil surrounding the sample. The sample was then placed in triaxial compression and deformed smoothly to an axial strain of between 10 and 14%. Axial load ($\sigma_1 - \sigma_3$) was monitored via an internal force gauge, radial deformation was monitored using the internal cantilever system, and axial deformation was monitored externally by recording the position of the loading ram via a linear displacement transducer. Confining pressure was monitored using a

Heise gauge and was held constant during the deformation of each sample. Differential axial load and axial and radial displacement were recorded using the multipurpose data acquisition system described in Section A4.

A3.2.2 Intermediate-Strain-Rate Tests

Tests to determine mechanical behavior at strain rates of 0.5 and 20 s^{-1} were conducted in the intermediate-strain-rate apparatus shown schematically in Fig. A7 and pictorially in Fig. A8. This apparatus used energy stored in a spinning flywheel to provide the force necessary for axial loading of the sample. Strain rate was varied by changing the speed of rotation of the flywheel that drives the piston loading cam. Test specimens 2.5 cm in diameter and 5.1 cm long were prepared in the same way as those used for pressure–volume testing (see Fig. A1). The sample was placed in the pressure vessel, and the vessel was assembled into the intermediate-rate apparatus. Argon gas was used as the confining medium for these tests. Each sample was tested by first introducing confining pressure and then applying axial load. Axial force was monitored by an internal force gauge placed in series with the sample. These data were recorded on a LeCroy modular waveform analyzer controlled by an IBM PC-XT computer. Data were later reduced using a SUN 3/50 workstation. Differential stress ($\sigma_1 - \sigma_3$) versus time was calculated by dividing the axial force data by the cross-sectional area of the sample. Axial displacement versus time was not measured directly for these tests. Axial displacement was calculated using the relation:

$$\Delta l = \omega \, (l/r) \, \Delta t,$$

where:

Δl = axial displacement in cm at time t,
ω = angular velocity of the shaft (radians/s),
l/r = rise in cam shaft per radian (cm/radian),
Δt = $t - t_0$ where t_0 = time at initiation of axial load.

The value ω was measured during each test.

A4. DATA ACQUISITION

Two different data-acquisition systems were used for these experiments. A multipurpose, 16-channel system was used for the uniaxial, pressure-volume, and triaxial tests at a strain rate of 10^{-4} s^{-1}. This system is shown schematically in Fig. A9 and pictorially in Fig. A10. Diagnostic signals are brought into a data distribution box via K-loc connectors and then carried via cable to an Analog Devices signal-conditioning module. This module provides conversion of various millivolt and volt signals into a signal in the range 0-10 volts which is then fed into a 16-channel, A/D board installed in an Apple Mac II computer. Data acquisition software was developed using the LabView program.

The data acquisition for the intermediate-rate tests included a LeCroy waveform digitizer that can sample at 1-μs intervals. The LeCroy was coupled to an IBM PC-XT. Data were reduced using a Sun 3/50 workstation (see Fig. A7).

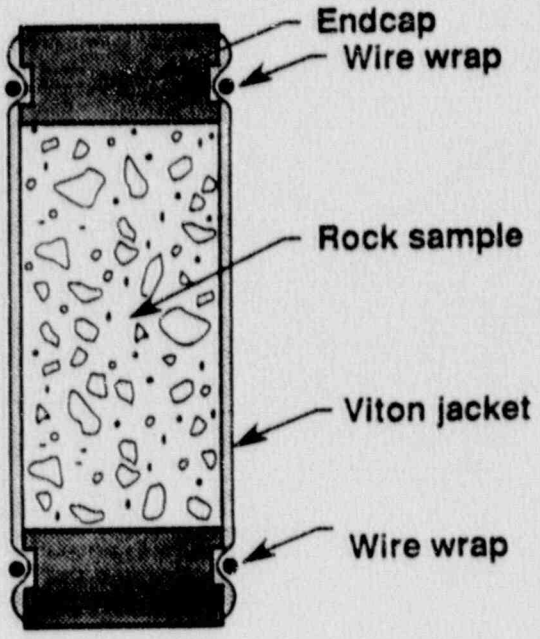

Fig. A1. Schematic of sample assembly for pressure-volume and confined compression tests.

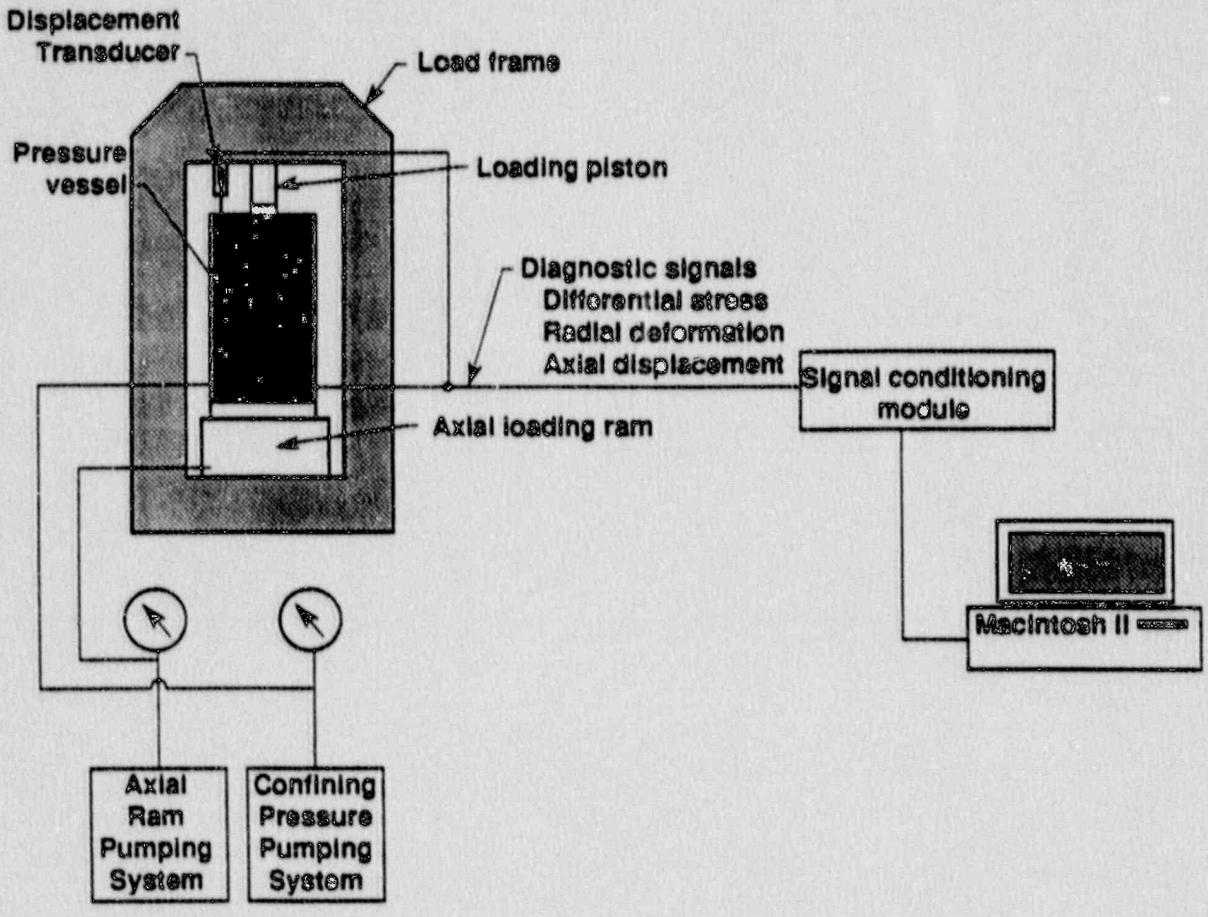

Fig. A2. Schematic of system used for pressure-volume and confined compression tests at a strain rate of 10^{-4} s^{-1}.

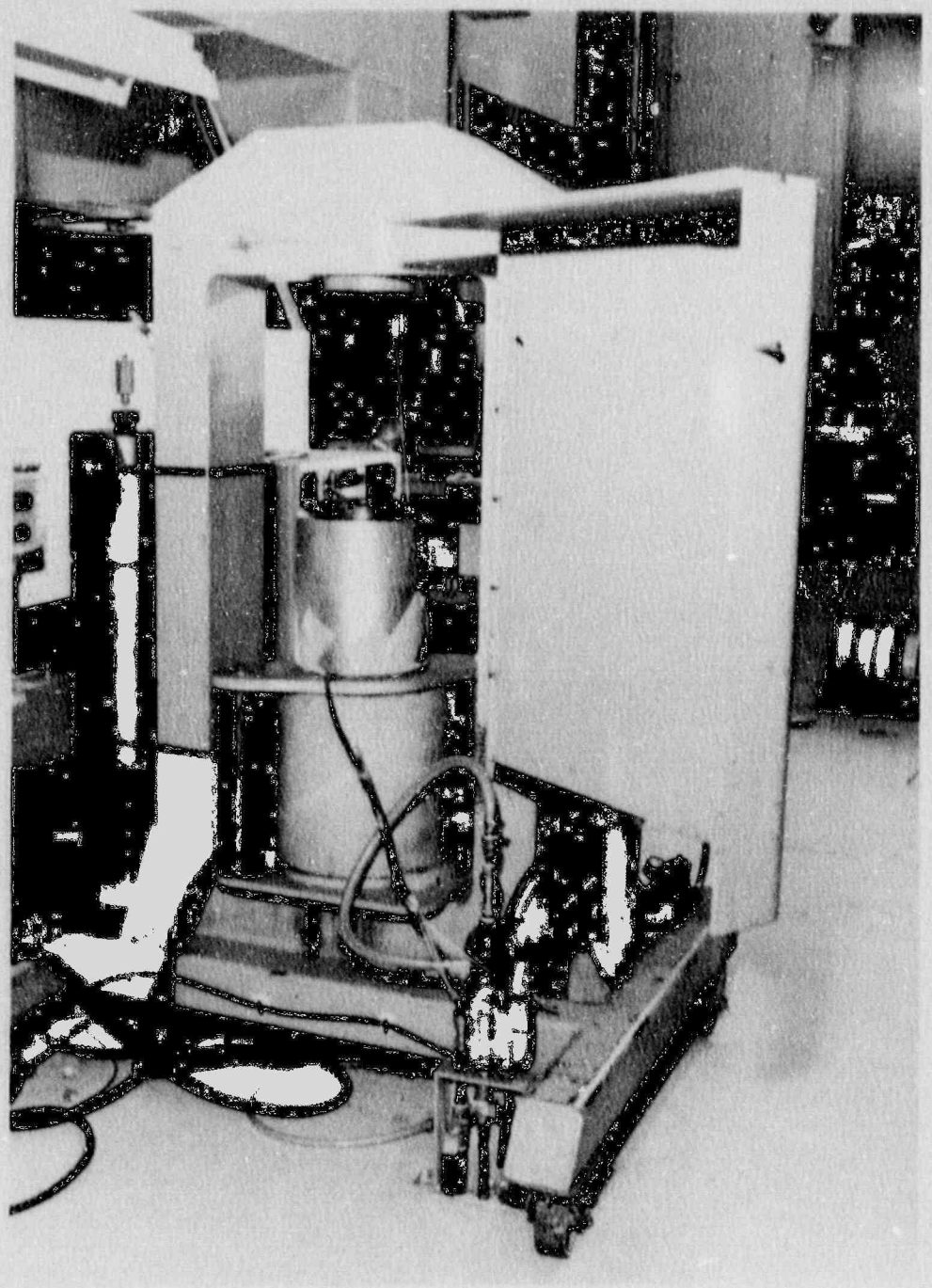

Fig. A3. Reaction frame used for pressure-volume and confined compression tests at a strain rate of 10^{-4} s^{-1}.

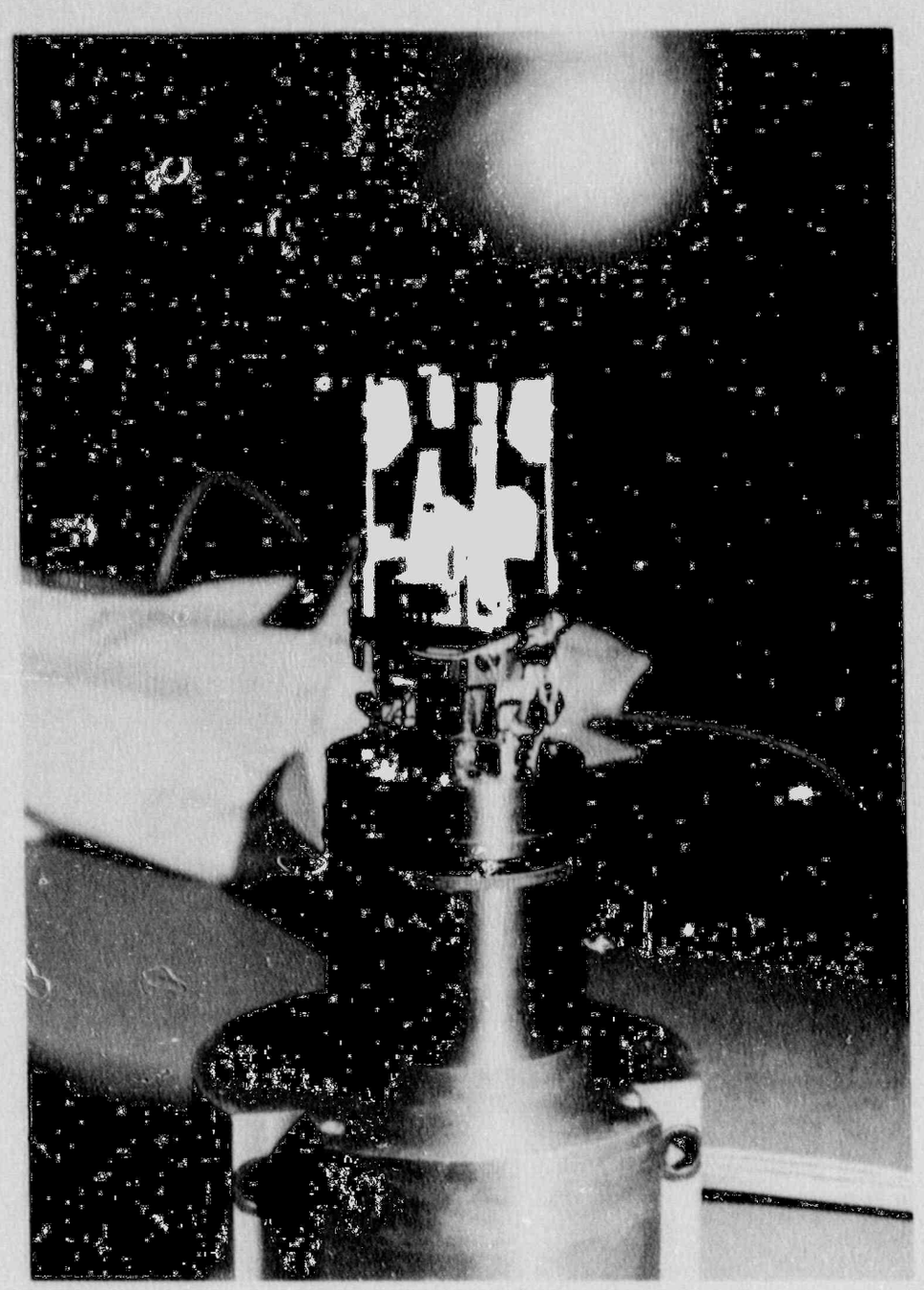

Fig. A4. Cantilever system used to monitor radial deformation.

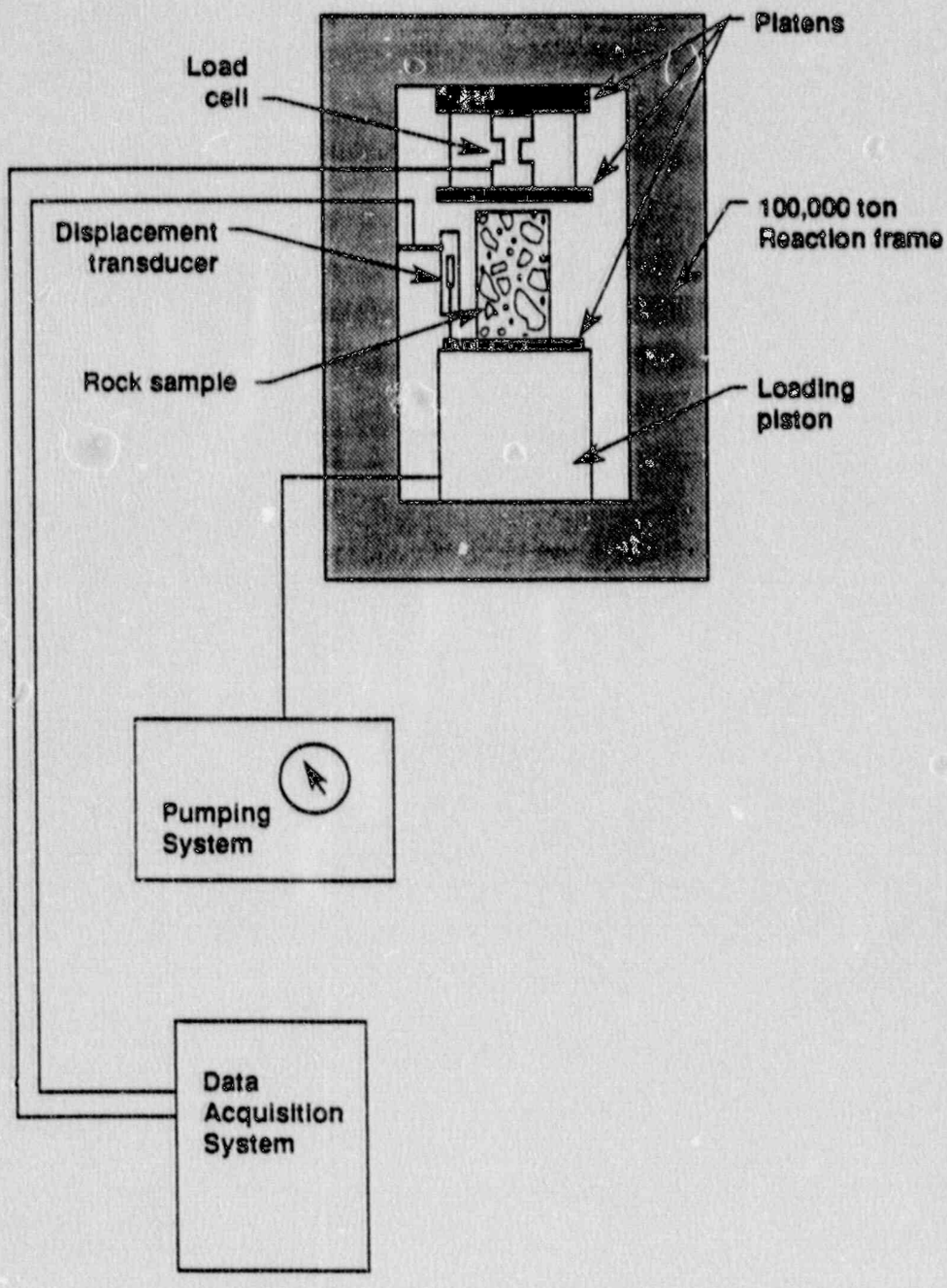

Fig. A5. Schematic of test system for uniaxial tests.

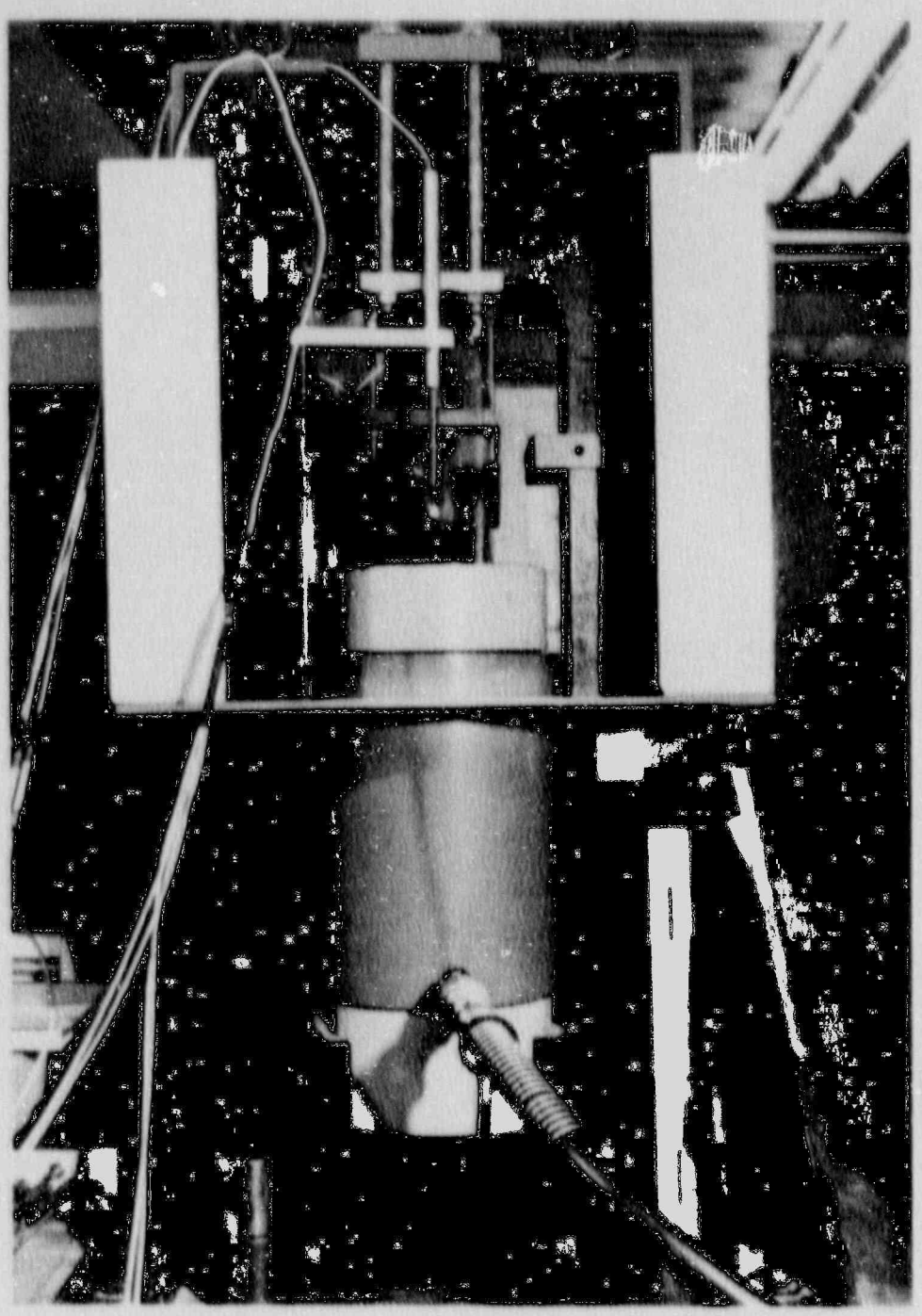

Fig. A6. Apparatus used for uniaxial tests.

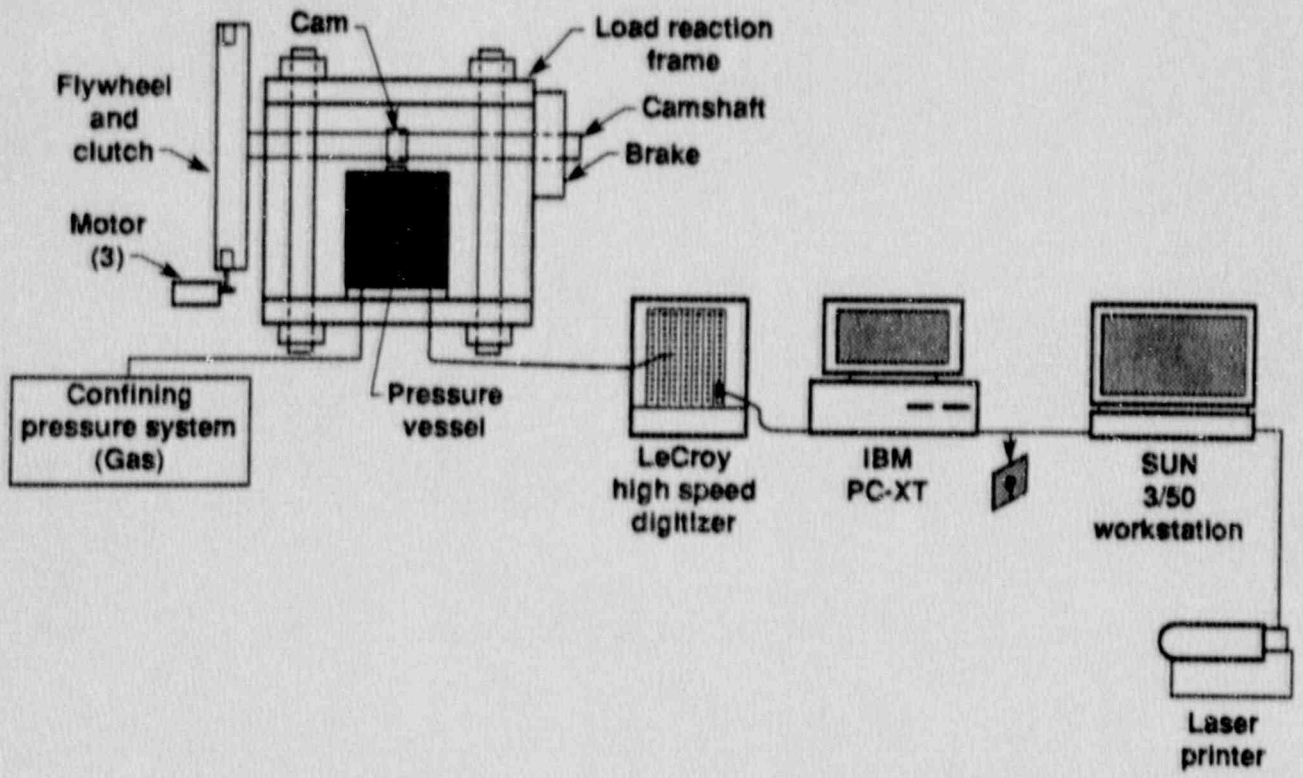

Fig. A7. Schematic of system used for intermediate-rate tests.

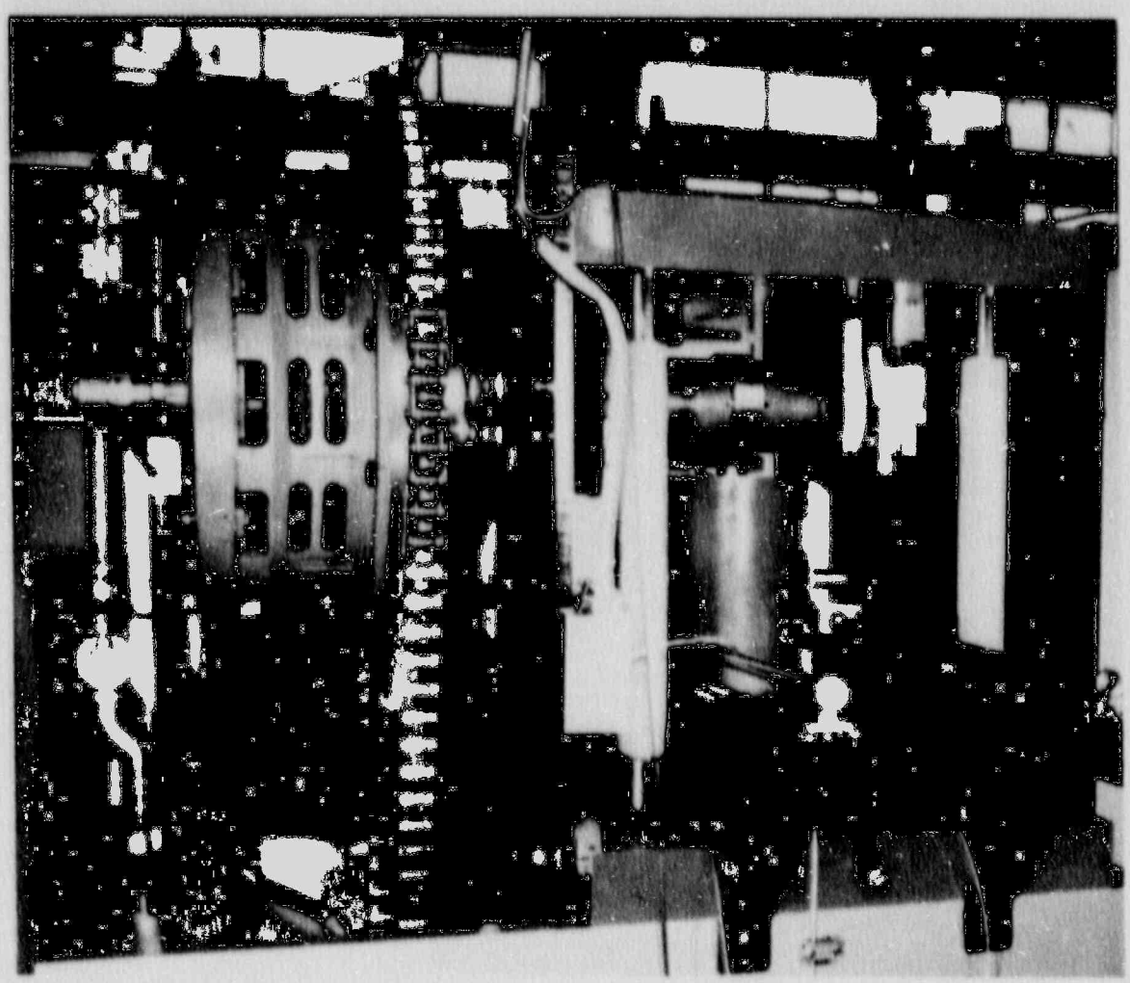

Fig. A8. Pictorial view of intermediate-rate apparatus.

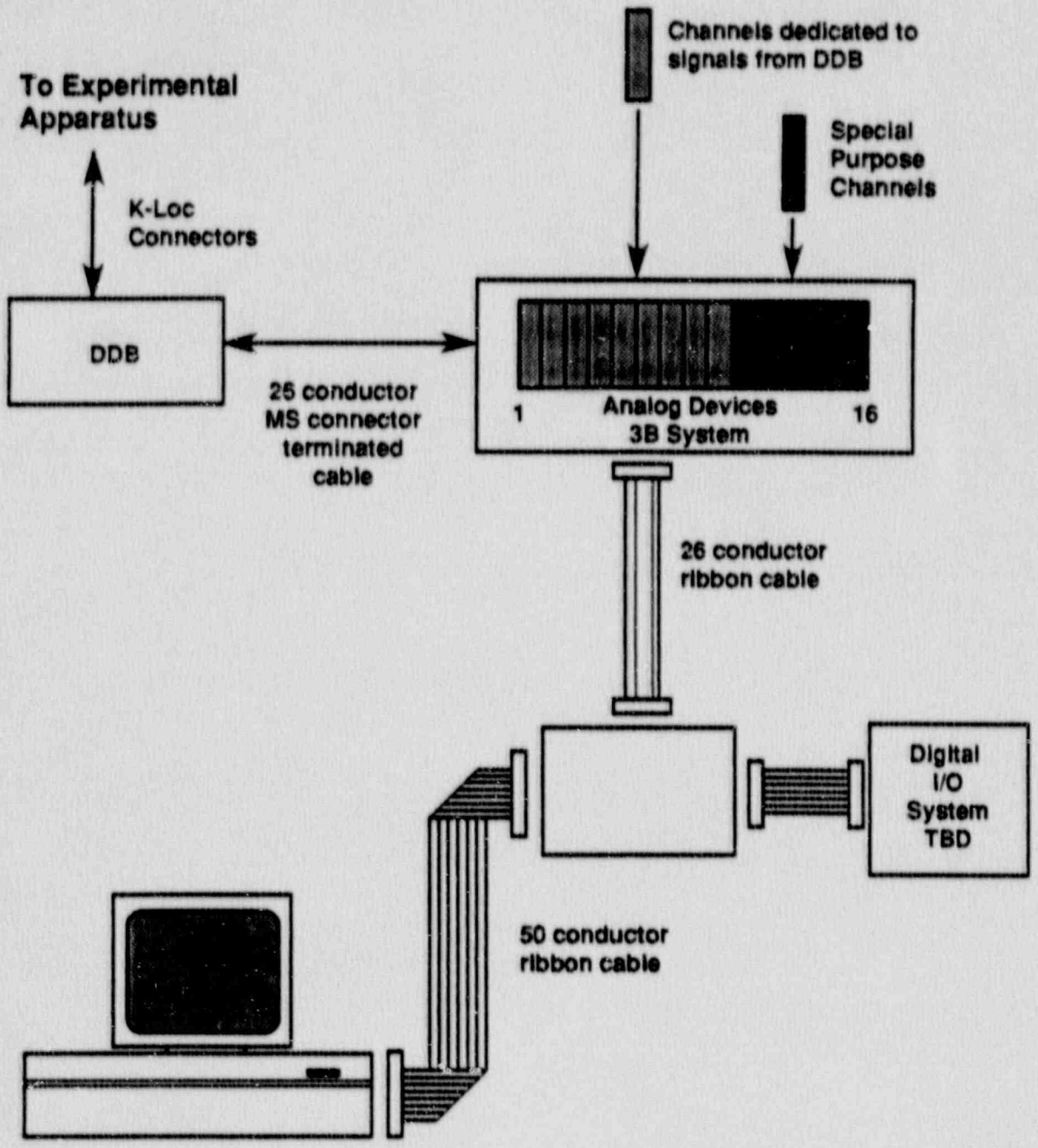

Fig. A9. Schematic of multipurpose digital data acquisition system.

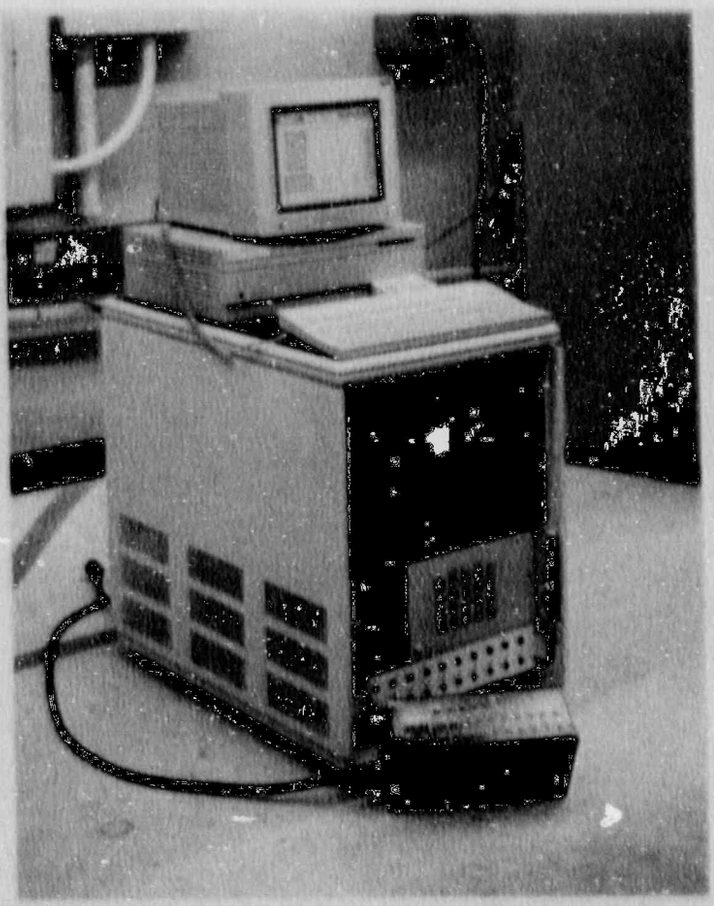

Fig. A10. Multipurpose digital data acquisition system.